4-19-2019

Stimulation of Heat Shock Protein 90 Chaperone Function Through Binding of a Novobiocin Analog KU-32

Bhaskar K. Chatterjee
From the Kusuma School of Biological Sciences.

Abhilash Jayaraj
the Supercomputing Facility for Bioinformatics and Computational Biology

Vinay Kumar
the Department of Chemistry, Indian Institute of Technology-Delhi, Hauz Khas

Brian Blagg
the Department of Medicinal Chemistry, University of Kansas

Rachel E. Davis
the Department of Medicinal Chemistry, University of Kansas

See next page for additional authors

Publication Info

The Journal of biological chemistry, Volume 294, Issue 16, 2019, pages 6450-6467.

Author(s)
Bhaskar K. Chatterjee, Abhilash Jayaraj, Vinay Kumar, Brian Blagg, Rachel E. Davis, B Jayaram, Shashank Deep, and Tapan K. Chaudhuri

Stimulation of heat shock protein 90 chaperone function through binding of a novobiocin analog KU-32

Received for publication, February 20, 2018, and in revised form, February 17, 2019 Published, Papers in Press, February 21, 2019, DOI 10.1074/jbc.RA118.002502

Bhaskar K. Chatterjee[‡], Abhilash Jayaraj[§1], Vinay Kumar[¶1,2], Brian Blagg[‖3], Rachel E. Davis[‖3], B. Jayaram[§], Shashank Deep[¶], and Tapan K. Chaudhuri[‡4]

From the [‡]Kusuma School of Biological Sciences, the [§]Supercomputing Facility for Bioinformatics and Computational Biology, and the [¶]Department of Chemistry, Indian Institute of Technology-Delhi, Hauz Khas, New Delhi 110016, India and the [‖]Department of Medicinal Chemistry, University of Kansas, Lawrence, Kansas 66045

Edited by Ursula Jakob

Heat shock protein 90 (Hsp90) is a eukaryotic chaperone responsible for the folding and functional activation of numerous client proteins, many of which are oncoproteins. Thus, Hsp90 inhibition has been intensely pursued, resulting in the development of many potential Hsp90 inhibitors, not all of which are well-characterized. Hsp90 inhibitors not only abrogate its chaperone functions, but also could help us gain insight into the structure–function relationship of this chaperone. Here, using biochemical and cell-based assays along with isothermal titration calorimetry, we investigate KU-32, a derivative of the Hsp90 inhibitor novobiocin (NB), for its ability to modulate Hsp90 chaperone function. Although NB and KU-32 differ only slightly in structure, we found that upon binding, they induce completely opposite conformational changes in Hsp90. We observed that NB and KU-32 both bind to the C-terminal domain of Hsp90, but surprisingly, KU-32 stimulated the chaperone functions of Hsp90 via allosteric modulation of its N-terminal domain, responsible for the chaperone's ATPase activity. *In vitro* and *in silico* studies indicated that upon KU-32 binding, Hsp90 undergoes global structural changes leading to the formation of a "partially closed" intermediate that selectively binds ATP and increases ATPase activity. We also report that KU-32 promotes HeLa cell survival and enhances the refolding of an Hsp90 substrate inside the cell. This discovery explains the effectiveness of KU-32 analogs in the management of neuropathies and may facilitate the design of molecules that promote cell survival by enhancing Hsp90 chaperone function and reducing the load of misfolded proteins in cells.

Hsp90 is a eukaryotic chaperone that plays a major role in protein homoeostasis under normal conditions (1). From aiding vesicular protein trafficking inside cells (2) to the formation of purinosome complexes within the nucleus (3), Hsp90 modulates diverse cellular activities. Under stress conditions, Hsp90 and other chaperones are overexpressed to aid in the prevention of apoptosis. The chaperones reduce the load of misfolded or unfolded intermediates as well as mediate the degradation of nonfunctional proteins via the ubiquitin-proteasome pathway (4). Hsp90 has over 200 client proteins, including the Raf kinase, Src family of tyrosine kinases (5), growth factor receptor tyrosine kinases like epidermal growth factor receptor and ErbB2 (6, 7), tumor suppressor protein p53 (8), and steroid hormone receptors (9). Most of these substrate proteins become oncogenic in certain types of cancer. Hence, abrogating Hsp90's chaperone function has been a major therapeutic paradigm for the treatment of cancer. Alternatively, treatment of the neurodegeneration observed in Alzheimer's disease and Parkinson's disease may require excessive levels or enhanced functionality of the chaperones, due to their cytoprotective role in preventing the accumulation of toxic oligomers like β-amyloid, Tau, and α-synuclein (10, 11).

Compounds that can inhibit the function of Hsp90 could be considered beneficial for the treatment of cancer, whereas those that can stimulate its function could be considered useful for treating neurodegenerative disorders. Thus, Hsp90 is considered a target for treating both cancer and neurodegenerative disorders. The development and characterization of compounds that modulate Hsp90's function through either of these mechanisms could be useful in the advancement of existing therapies targeting cancer and neurodegeneration.

There are two major classes of Hsp90 inhibitors: those that bind to the N-terminal domain (NTD)[5] and those that bind to the C-terminal domain (CTD) (12). Most NTD inhibitors, such as geldanamycin (GA) and radicicol prevent Hsp90 from hydrolyzing ATP by competitively inhibiting the binding of ATP to the NTD of Hsp90 and thereby stall the ATP-dependent Hsp90 protein-folding cycle (12, 13). Most CTD inhibitors, such as NB, epigallocatechin gallate, and taxol exert their inhibitory effect by allosterically regulating NTD's function,

The authors declare that they have no conflicts of interest with the contents of this article.

This article contains Tables S1–S5 and Figs. S1–S19.

[1] Both authors contributed equally to this work.

[2] Present address: Clensta International Private Ltd., FITT-BBIF-Bldg., Indian Institute of Technology-Delhi, Hauz Khas, New Delhi 110016.

[3] Present address: Dept. of Chemistry and Biochemistry, University of Notre Dame, Notre Dame, IN 46554.

[4] To whom correspondence should be addressed: Kusuma School of Biological Sciences, Indian Institute of Technology-Delhi, Hauz Khas, New Delhi 110016, India. Tel.: 91-2659-1012; Fax: 91-2659-7530; E-mail: tkchaudhuri@bioschool.iitd.ac.in.

[5] The abbreviations used are: NTD, N-terminal domain; CTD, C-terminal domain; hHsp90, human Hsp90; GA, geldanamycin; NB, novobiocin; MD, molecular dynamics; RMSD, root mean square deviation; PDB, Protein Data Bank; DRI, dose reduction index; CI, combination index; f_a, fraction of cells affected by compound(s); 3D, three-dimensional; MTT, 3-(4,5-dimethylthiazol-2-yl)-2,5-diphenyltetrazolium bromide; ANOVA, analysis of variance; PK/LDH, pyruvate kinase/lactate dehydrogenase.

most likely through movement of Hsp90's middle domain (14). Other CTD inhibitors exert their inhibitory effect by disrupting co-chaperone binding to Hsp90 (15). Studies have shown that NB prebound to Hsp90 prevents GA binding, whereas saturating concentrations of GA do not exert any effect on NB binding (15, 16). These studies led to a general understanding that small-molecule binding occurs at both of the domains and that compounds bound to the CTD influence the binding of ATP and inhibitors to the NTD (18, 19). Although many co-crystal structures of ATP inhibitors bound to the NTD have been solved (20), little structural information is available for the CTD. Some studies claim that the CTD is responsible for Hsp90 dimerization and the binding of many important co-chaperones (14). Thus, compounds that bind to the CTD and interfere with these essential functions may be more effective at inhibiting the Hsp90 chaperone machinery than NTD inhibitors. The "KU" series of compounds are synthetic NB derivatives that exhibit improved binding affinity for the Hsp90 CTD and manifest increased anti-proliferative activity relative to NB (21–24). KU-32, however, was observed to behave as a neuroprotective agent in the treatment of diabetic peripheral neuropathy and did not exert any adverse effect on pancreatic islets (25, 26).

The present study was designed to utilize biochemical and cell-based assays to determine how KU-32 modulates the function of Hsp90 differently than its parent compound NB. *In silico* studies were carried out to identify potential variations within local structural modulations induced by the binding of KU-32 and NB and to identify their impact on the global structural dynamics of Hsp90. Furthermore, combinatorial studies utilizing both an NTD inhibitor (GA) and a CTD binder (NB or KU-32) were carried out to investigate their simultaneous binding events and whether allosteric constraints would modulate their binding and subsequent effect on chaperone function.

Results

KU-32 stimulates the ATPase activity of Hsp90, whereas GA and NB act as inhibitors

ATP hydrolysis plays a key role in the chaperone cycle of Hsp90 by providing the requisite energy for nascent or partially folded polypeptides to acquire their functional conformation upon undergoing multiple cycles of binding and release (27, 28). KU-32's role in the Hsp90 ATPase cycle was determined using the PK/LDH coupled assay. Binding of KU-32 to human His-tagged recombinant Hsp90 increased ATP turnover rates when compared with the ATPase activity of Hsp90 alone, with the greatest stimulation (~69%) occurring at 1:1 (Hsp90 monomer/KU-32) molar ratio. At the highest KU-32 concentration of 90 μM, ATPase activity increased by 35% (Table 1 and Fig. S1*c*). Compared with KU-32, NB exhibited a basal rate of inhibition and reduced the ATPase activity by 40% and ~50% at its lowest and highest concentrations, respectively (Table 1 and Fig. S1*b*). GA, a previously reported Hsp90 ATPase inhibitor (29), inhibited the ATPase activity in a dose-dependent fashion, with the lowest and highest GA concentration reducing the ATPase activity by ~59 and 81%, as compared with control studies (Table 1 and Fig. S1*a*). These observations suggest that KU-32 stimulates Hsp90 ATPase activity, whereas GA and NB act as inhibitors.

Table 1
ATP hydrolysis rates of human Hsp90β in the presence of a single compound or a combination of compounds

Row 1 indicates the ATPase rate of 6 μM Hsp90 in the absence of any compounds. Rows 2–4 indicate the ATPase rates of 6 μM Hsp90 in the presence of compounds acting alone. Combinatorial studies (rows 5 and 6) were carried out by incubating 6 μM Hsp90 with 6 μM GA and 90 μM of either NB or KU-32. Right arrows represent the sequence of the addition of the compounds to the Hsp90-containing buffer. Plus signs represent a mixture of two compounds. *, unpaired two-tailed *t* tests to evaluate significant differences between ATPase rates obtained in the presence of compounds acting alone and in combination yielded *p* values < 0.01 in all cases except *a* ($p = 0.01$), *b* ($p = 0.04$), and *c* ($p = 0.08$), where marginal or no significant differences were observed.

Compounds acting alone or in combination	Concentrations of compounds used (μM)	ATPase rate
		$min^{-1}\ \mu M^{-1}$ *Hsp90*
Hsp90	6	0.097 ± 0.002
GA	6	0.040 ± 0.003
	30	0.034 ± 0.002
	60	0.027 ± 0.001
	90	0.018 ± 0.002
NB	6	0.058 ± 0.002
	30	0.055 ± 0.001
	60	0.047 ± 0.003
	90	0.050 ± 0.001
KU-32	6	0.164 ± 0.006
	30	0.148 ± 0.006
	60	0.150 ± 0.005
	90	0.131 ± 0.006
(GA and NB)*	GA → NB	0.029 ± 0.001
	NB → GA	0.027 ± 0.001
	GA + NB	0.028 ± 0.001
(GA and KU-32)*	GA → KU-32[a]	0.115 ± 0.008
	KU-32 → GA[b]	0.120 ± 0.008
	KU-32 + GA[c]	0.123 ± 0.007

C-terminal binders modulate GA-mediated inhibition of Hsp90 ATPase activity

To understand whether NTD and CTD binders allosterically regulate the binding of one another and thus modulate Hsp90 ATPase activity, we conducted studies that included a combination of either GA/NB or GA/KU-32. Each study was carried out in three different ways: Hsp90 incubated with GA followed by further incubation with either NB or KU-32; Hsp90 incubated with either NB or KU-32 followed by further incubation with GA; and Hsp90 incubated with a mixture containing either GA and NB or GA and KU-32. All three conditions under which GA and NB were combined reduced the ATPase activity by ~72% and therefore exhibited a slightly greater degree of ATPase inhibition relative to either GA (6 μM) or NB (90 μM) alone (Table 1, Fig. 1 (*a* and *b*), and Fig. S1*e*). Interestingly, KU-32, when combined with GA, interfered with GA-mediated ATPase inhibition and manifested a similar effect as KU-32 alone, exhibiting a 26% increase in the ATPase activity of Hsp90 (Table 1, Fig. 1 (*a* and *b*), and Fig. S1*d*). These observations suggest that NB appeared to partially complement GA-mediated ATPase inhibition, whereas KU-32 appeared to antagonize the inhibitory function of GA.

N- and C-terminal binders differentially modulate ATP binding to the N terminus of Hsp90

ATP binding is a precursor to ATP hydrolysis; therefore, isothermal titration calorimetry studies were performed to further

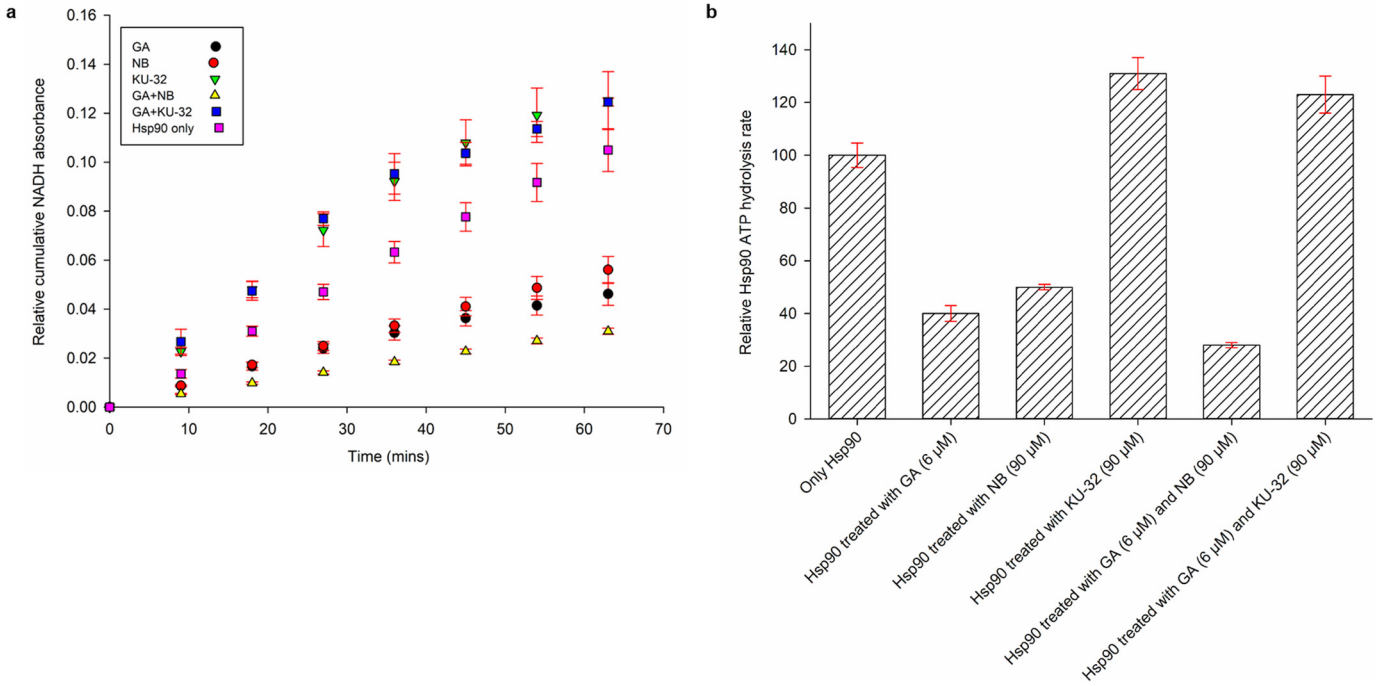

Figure 1. ATPase activity of Hsp90. *a*, hydrolysis of ATP by 6 μM Hsp90 was monitored for 60 min by measuring the relative cumulative NADH absorbance at 340 nm. ATP hydrolysis was then monitored in the presence of GA (6 μM), NB (90 μM), and KU-32 (90 μM). Finally, ATP hydrolysis was monitored when 6 μM GA was combined with either 90 μM NB or KU-32. GA + NB and GA + KU-32 signify that mixtures of these compounds were separately prepared and then added to a reaction mixture containing Hsp90. *b*, bar graph depicting ATP hydrolysis rates of Hsp90 in the presence of GA, NB, and KU-32 acting alone or in combination relative to Hsp90 acting alone. *Error bars*, S.D.

Table 2

Thermodynamic parameters of small molecules binding to Hsp90 alone

20 μM recombinant human Hsp90β was titrated against 0.1 mM GA, NB, or KU-32 (rows 1–3, respectively), 1 mM ATP (row 4), and 1 mM ADP (row 5).

Compounds titrated against Hsp90 alone	K_d	$T\Delta S$	ΔH	ΔG
	μM	kcal/mol	kcal/mol	kcal/mol
GA	0.25 ± 0.01	0.42 ± 0.02	−4.06 ± 0.10	−4.48 ± 0.12
NB	1.01 ± 0.02	0.61 ± 0.03	−0.90 ± 0.01	−1.51 ± 0.04
KU-32	0.21 ± 0.04	0.29 ± 0.02	−4.9 ± 0.30	−5.19 ± 0.32
ATP	41.2 ± 3.50	0.39 ± 0.02	−1.39 ± 0.25	−1.78 ± 0.27
ADP	2.38 ± 0.04	−0.2 ± 0.02	−10 ± 0.97	−9.80 ± 0.95

assist in the interpretation of the results obtained from ATPase experiments. The binding affinities of small-molecule binders of Hsp90 were determined. Binding of KU-32 and GA were enthalpy-driven, whereas the binding of NB was driven by both favorable entropy and favorable enthalpy in almost equal quantities (Table 2 and Fig. 2 (*a*–*c*). Binding reactions of ADP and ATP to Hsp90 were primarily enthalpy-driven (Table 2 and Fig. 2 (*d* and *e*)). ADP bound Hsp90 with ~17 times higher affinity as compared with ATP. The enthalpy and Gibbs free energy of ADP binding, respectively, were ~7.2 times and ~5.5 times higher than those of ATP binding. This indicates that ADP binds Hsp90 more spontaneously than ATP. To investigate the effect of Hsp90 binders on the binding of ATP to the NTD, ATP was titrated against Hsp90 preincubated with either GA, NB, or KU-32. As expected, GA abrogated ATP binding, as evidenced by an ~80 times increase in the K_d value (Table 3 and Fig. 3*a*). The enthalpy and entropy of ATP binding to the Hsp90–GA complex decreased by ~93 and ~75%, respectively, as compared with ATP binding to Hsp90 alone. NB has been previously shown to allosterically inhibit ATP binding to the NTD of Hsp90 (16). Our studies also indicate that the Hsp90–NB complex did not bind ATP, as evidenced by a K_d value of ~3000 μM (Table 3 and Fig. 3*b*). Conversely, KU-32 did not adversely affect the binding of ATP to Hsp90. In fact, ATP bound the Hsp90–KU-32 complex with an enthalpy-driven affinity very similar to that for Hsp90 alone (Table 3 and Fig. 3*c*).

To determine how ATP binding was affected in the presence of a combination of NTD and CTD binders together, ATP was titrated against Hsp90–GA–KU-32 and Hsp90–GA–NB complexes. In accordance with our ATPase results, ATP bound the Hsp90–GA–KU-32 complex with an enthalpy-driven affinity similar to that of the Hsp90–KU-32 complex (Table 3 and Fig. 3*e*). ATP titration against a Hsp90–GA–NB complex showed further reduction in ATP binding with respect to the Hsp90–GA and Hsp90–NB complexes (Table 3 and Fig. 3*d*). This binding event was entropy-driven with little contribution from enthalpy and indicated the formation of a random state that does not favor ATP binding. Taken together, these observations suggest that NB and GA act as inhibitors of chaperone function by preventing ATP binding and subsequent hydrolysis. Furthermore, they appear to behave as agonists as our ATPase results had previously indicated. Additionally, ATP-binding affinities for the Hsp90–KU-32 and Hsp90–GA–KU-32 complexes suggest that KU-32 binding induces conformational changes in the NTD of Hsp90 that favor the binding of ATP but not GA.

N- and C-terminal binders allosterically modulate binding of one another to the Hsp90 C and N terminus

Titration studies were carried out to enhance our understanding of the ATPase results (obtained when compounds

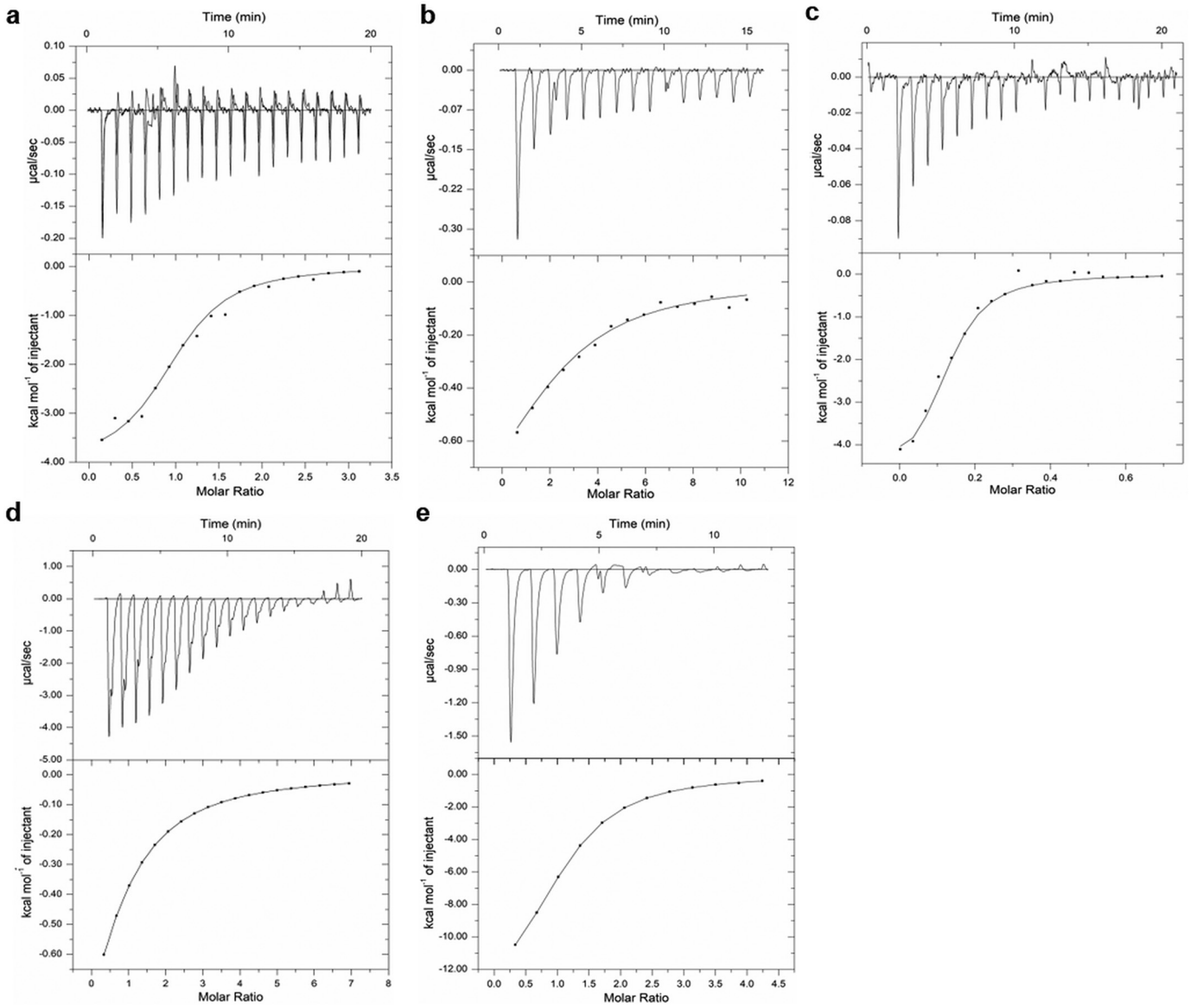

Figure 2. Titration of small molecules against Hsp90. 20 μM recombinant human Hsp90β was titrated against 0.1 mM GA (*a*), 0.1 mM NB (*b*), and 0.1 mM KU-32 (*c*). 30 μM Hsp90β was titrated against 1 mM ATP (*d*) and 1 mM ADP (*e*). The heat of binding was calculated after subtracting the heat of dilution from control experiments where GA, NB, KU-32, ATP, and ADP were titrated against reaction buffer only.

Table 3

Thermodynamic parameters of ATP binding to Hsp90–small molecule complexes

30 μM recombinant human Hsp90β was mixed with an equimolar amount of either GA, NB, or KU-32 (rows 1–3, respectively) and then titrated against 1 mM ATP. A mixture containing either 30 μM GA and 30 μM NB (row 4) or 30 μM GA and 30 μM KU-32 (row 5) was added to the buffer containing 30 μM Hsp90, and the resultant mixture was titrated against 1 mM ATP. Unpaired two-tailed *t* tests to evaluate significant differences among binding affinities of ATP obtained when titrated against Hsp90 alone, Hsp90–GA/NB/KU-32 complexes, Hsp90 + GA + NB, and Hsp90 + GA + KU-32 yielded p values < 0.05 in all cases except *a* ($p = 0.98$), *b* ($p = 0.76$), and # ($p = 0.45$), where no significant differences were observed.

Hsp90 – compound complex titrated against ATP	K_d	$T\Delta S$	ΔH	ΔG
	μM	*kcal/mol*	*kcal/mol*	*kcal/mol*
Hsp90 + GA	3333.3 ± 19.6	0.1 ± 0.01	−0.1 ± 0.07	−0.23 ± 0.08
Hsp90 + NB	2879 ± 17.4	0.14 ± 0.03	−0.12 ± 0.02	−0.26 ± 0.05
Hsp90 + KU-32[a,#]	36.8 ± 2.16	0.38 ± 0.02	−1.51 ± 0.23	−1.89 ± 0.25
Hsp90 + GA + NB	10^4 ± 120	0.21 ± 0.02	−0.09 ± 0.01	−0.30 ± 0.03
Hsp90 + GA + KU-32[b,#]	50 ± 3.45	0.38 ± 0.03	−1.41 ± 0.02	−1.79 ± 0.05

were sequentially incubated with Hsp90) and to investigate whether the binding of one compound to the CTD of Hsp90 allosterically modulated the binding of a second compound to the NTD and vice versa. The binding affinity of GA for the Hsp90–KU-32 complex was drastically reduced as compared with Hsp90 alone (K_d of 52.9 μM *versus* 0.25 μM). The binding event exhibited both unfavorable entropy (~340%) and enthalpy (~60%) as compared with the binding of GA to Hsp90 alone (Table 4 and Fig. S2*a*). KU-32 and NB both bound the Hsp90–GA complex with reduced affinities compared with

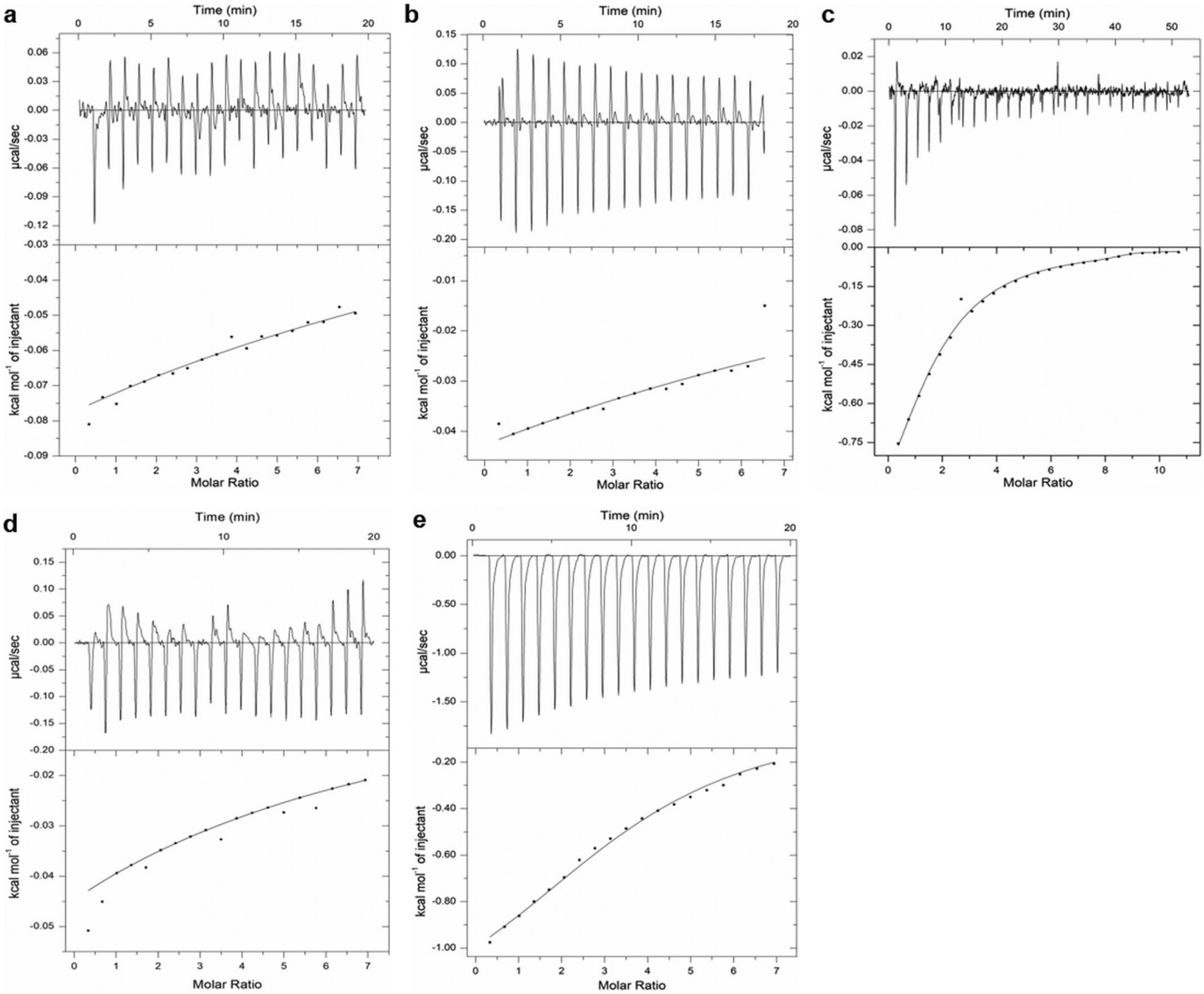

Figure 3. ATP titration against Hsp90 bound to individual compounds and their combinations. 1 mM ATP was titrated against 30 μM recombinant human Hsp90β preincubated with 30 μM GA (*a*), 30 μM NB (*b*), 30 μM KU-32 (*c*), 30 μM GA and 30 μM NB (*d*), and 30 μM GA and 30 μM KU-32 (*e*). The heat of binding was calculated after subtracting the heat of dilution from control experiments where 1 mM ATP was titrated against reaction buffer containing only compound(s).

Table 4

Thermodynamic parameters of NTD and CTD binders binding to various Hsp90–NTD or Hsp90–CTD complexes

Row 1 indicates the titration of 0.1 mM NB against a complex of 20 μM Hsp90β and 20 μM GA (represented as GA^c). Row 2 indicates the titration of 0.1 mM GA against a complex of 20 μM Hsp90β and 20 μM NB (represented as NB^c). Row 3 indicates the titration of 0.1 mM GA against a complex of 20 μM Hsp90β and 20 μM GA (represented as KU-32^c). Row 4 indicates the titration of 0.1 mM KU-32 against a complex of 20 μM Hsp90β and 20 μM GA (represented as GA^c). Row 5 indicates the titration of 0.1 mM NB against a complex of 20 μM Hsp90β and 20 μM KU-32 (represented as KU-32^c). Unpaired two-tailed *t* tests to evaluate significant differences between binding affinities of GA obtained when titrated against Hsp90 alone and Hsp90–NB/Hsp90–KU-32 complexes; between binding affinities of NB obtained when titrated against Hsp90 alone and Hsp90–GA/ Hsp90–KU-32 complexes; and between binding affinities of KU-32 obtained when titrated against Hsp90 alone and Hsp90–GA complex yielded p values < 0.05 in all cases.

Compounds titrated against other Hsp90 – compound complexes	K_d	$T\Delta S$	ΔH	ΔG
	μM	*kcal/mol*	*kcal/mol*	*kcal/mol*
GA^c/NB	9.9 ± 0.74	0.14 ± 0.03	−5.2 ± 0.67	−5.34 ± 0.07
NB^c/GA	30.1 ± 6.80	−0.03 ± 0.01	−0.96 ± 0.09	−0.93 ± 0.09
KU-32^c/GA	52.9 ± 6.35	−0.99 ± 0.08	−1.76 ± 0.20	−0.77 ± 0.12
GA^c/KU-32	4.03 ± 0.62	0.003	−7.31 ± 0.94	−7.31 ± 0.94
KU-32^c/NB	102.5 ± 3.60	−0.9 ± 0.10	−1.07 ± 0.14	−0.17 ± 0.04

Hsp90 alone, as evidenced by the K_d values of 4 and 10 μM, respectively. These binding reactions were both entirely enthalpy-driven (Table 4 and Figs. S2*b* and S3*a*). The binding affinity of GA for the Hsp90–NB complex was drastically reduced as compared with Hsp90 alone (K_d of ~30 μM *versus* 0.25 μM, respectively). The binding event was enthalpy-driven, and both ΔG and ΔH were reduced as compared with the binding reaction of GA to Hsp90 alone (Table 4 and Fig. S3*b*). NB and KU-32 reduced the binding affinity of GA by ~120 and ~200 times, respectively, whereas GA reduced the binding affinities of NB

Table 5

Thermodynamic parameters of adenosine nucleotides binding to Hsp90–small molecule complexes

Row 1 indicates the titration of 1 mM ADP against 30 μM Hsp90β preincubated with 30 μM KU-32. Row 2 indicates the titration of 1 mM ATP against 30 μM Hsp90β preincubated sequentially with 30 μM KU-32 and 30 μM ADP. Row 3 indicates the titration of 0.15 mM ADP against 30 μM Hsp90β preincubated with 30 μM GA. Row 4 indicates the titration of 30 μM Hsp90β preincubated with 30 μM NB against 1 mM ADP. Row 5 indicates the titration of 30 μM Hsp90β preincubated with 30 μM GA against 1 mM ADP. Unpaired two-tailed t tests to evaluate significant differences between binding affinities of ADP obtained when titrated against Hsp90 alone and Hsp90–GA/NB/KU-32 complexes yielded p values < 0.05 in all cases except # ($p = 0.99$), where no significant difference was observed. A similar test carried out between binding affinities of ATP obtained when titrated against Hsp90 alone and the Hsp90-KU-32-ADP complex yielded a p value < 0.05.

Hsp90 – compound complex	+ADP				+ATP			
	K_d	$T\Delta S$	ΔH	ΔG	K_d	$T\Delta S$	ΔH	ΔG
	μM	kcal/mol	kcal/mol	kcal/mol	μM	kcal/mol	kcal/mol	kcal/mol
(Hsp90 + KU-32)#	10 ± 1	−0.69 ± 0.04	−15.9 ± 1.70	−15.21 ± 1.66				
(Hsp90 + KU-32) + ADP					5.65 ± 0.48	0.50 ± 0.07	−1.20 ± 0.26	−1.70 ± 0.17
(Hsp90 + GA)								
(Hsp90 + NB)#	10.1 ± 1.33	−0.33 ± 0.03	−10.7 ± 0.65	−10.37 ± 0.62				
(Hsp90 + GA)	3.23 ± 0.46	0.33 ± 0.05	−3.6 ± 0.45	−3.93 ± 0.50				

and KU-32 by ~10 and ~20 times, respectively. These observations indicated negative allosteric cross-talk between both of the Hsp90's termini, with the function of NTD being more strongly regulated by the CTD.

KU-32 lowers the binding affinity of ADP to Hsp90

ADP release is essential for Hsp90 to re-enter its catalytic cycle following ATP hydrolysis, and hence, we wanted to determine whether KU-32 played a role in ADP binding and its subsequent release. ADP binding to the Hsp90–KU-32 complex was enthalpy-driven and manifested an increase in the K_d value (10 μM) as compared with ADP binding to Hsp90 alone (Table 5 and Fig. 4*a*). Reduced binding affinity of ADP to Hsp90 might have an impact on ATP binding to the Hsp90–KU-32–ADP complex and could indirectly indicate ADP release. ATP bound the Hsp90–KU-32–ADP complex with ~7 times higher affinity as compared with Hsp90 alone. The binding reaction was enthalpy-driven, and the thermodynamic parameters of binding were similar to ATP binding to Hsp90 alone (Table 5 and Fig. 4*b*). This indicates that the conformation of the Hsp90 NTD in complex with KU-32 favors ADP release and subsequent ATP binding.

GA annuls whereas NB slightly reduces ADP binding to Hsp90

Additional titration experiments were carried out to study the effect of Hsp90 inhibitors GA and NB on ADP binding to the NTD of Hsp90 and determine whether they modulate the binding of ADP and ATP differently. ADP at a concentration of 0.15 mM was unable to bind the Hsp90–GA complex (Table 5 and Fig. S4*a*). This observation is in accordance with the fact that the binding affinity of GA to the NTD of Hsp90 is higher than that of ADP. However, ADP was able to bind the Hsp90–GA complex when titrated at a concentration of 1 mM (Table 5 and Fig. S4*b*). The reaction was enthalpy-driven, and ADP bound the Hsp90–GA complex with a similar affinity as compared with ADP binding to Hsp90 alone. This could happen when the difference in concentration between two ligands (ADP and GA) sharing the same binding site far exceeds the difference in their K_d value. This means that even though the binding affinity of GA to Hsp90 is ~10 times higher than that of ADP, a ~30 times excess of ADP can displace GA from its binding site. To determine whether the CTD inhibitor NB allosterically affects ADP binding to the NTD of Hsp90, a preformed Hsp90–NB complex was titrated against 1 mM ADP. ADP was able to bind the Hsp90–NB complex with a slightly reduced binding affinity as compared with ADP binding to Hsp90 alone (K_d ~10 μM). The binding was enthalpy-driven, and the thermodynamic parameters of binding were observed to be similar to those of ADP titrated against the Hsp90–KU-32 complex (Table 5 and Fig. S5). This was a surprising observation as, unlike ADP, the binding affinities of ATP and GA were drastically reduced when Hsp90 was prebound to NB. It would be interesting to study the conformational changes that occur in the NTD upon KU-32 and NB binding and how these structural changes affect the accessibility of the NTD nucleotide-binding cleft.

Hsp90 adopts a partially closed conformation upon KU-32 binding

Docking and molecular dynamics (MD) simulation studies were carried out to observe structural perturbations that occur upon KU-32 binding to Hsp90 and understand the contrasting effects of KU-32 and NB on Hsp90's function. The modeled Hsp90β dimer structure (Fig. S6) was in complete agreement with its closed counterpart (30). Each of the four compounds (ATP, GA, NB, and KU-32) was docked, and their ΔG of binding was calculated (Table S1). In agreement with our ITC studies, KU-32 bound Hsp90 more spontaneously than NB at the CTD. ATP bound to NTD of the modeled Hsp90β (Fig. S7*a*) had an RMSD of 1.67 Å as compared with the Hsp90α–ATP complex (PDB code 3T0Z). The Hsp90β–GA complex (Fig. S7*c*) had an RMSD of 1.54 Å as compared with the Hsp90α–GA complex (PDB code 1YET). The docking poses of NB and KU-32 bound to Hsp90 are depicted in Fig. S7 (*b* and *d*). The Hsp90 residues that interacted with KU-32 have been depicted in Fig. S7*e*. Our docking studies indicated that KU-32 and NB bound at a similar location within the CTD even though their interacting residues were different. This observation was further confirmed by titrating NB against a preformed Hsp90–KU-32 complex. (Table 4 and Fig. S8). As expected, the binding affinity of NB to this complex was drastically reduced, as evidenced by a K_d of ~100 μM.

To understand the divergent behavior of NB and KU-32 at an atomic resolution, MD simulations were performed with the modeled free Hsp90β or Hsp90β bound to KU-32 (alone or with ATP bound at the NTD) or NB (Table S2). No significant structural changes were observed for the unbound Hsp90 and the Hsp90–NB complex. MD simulation of the Hsp90–KU-

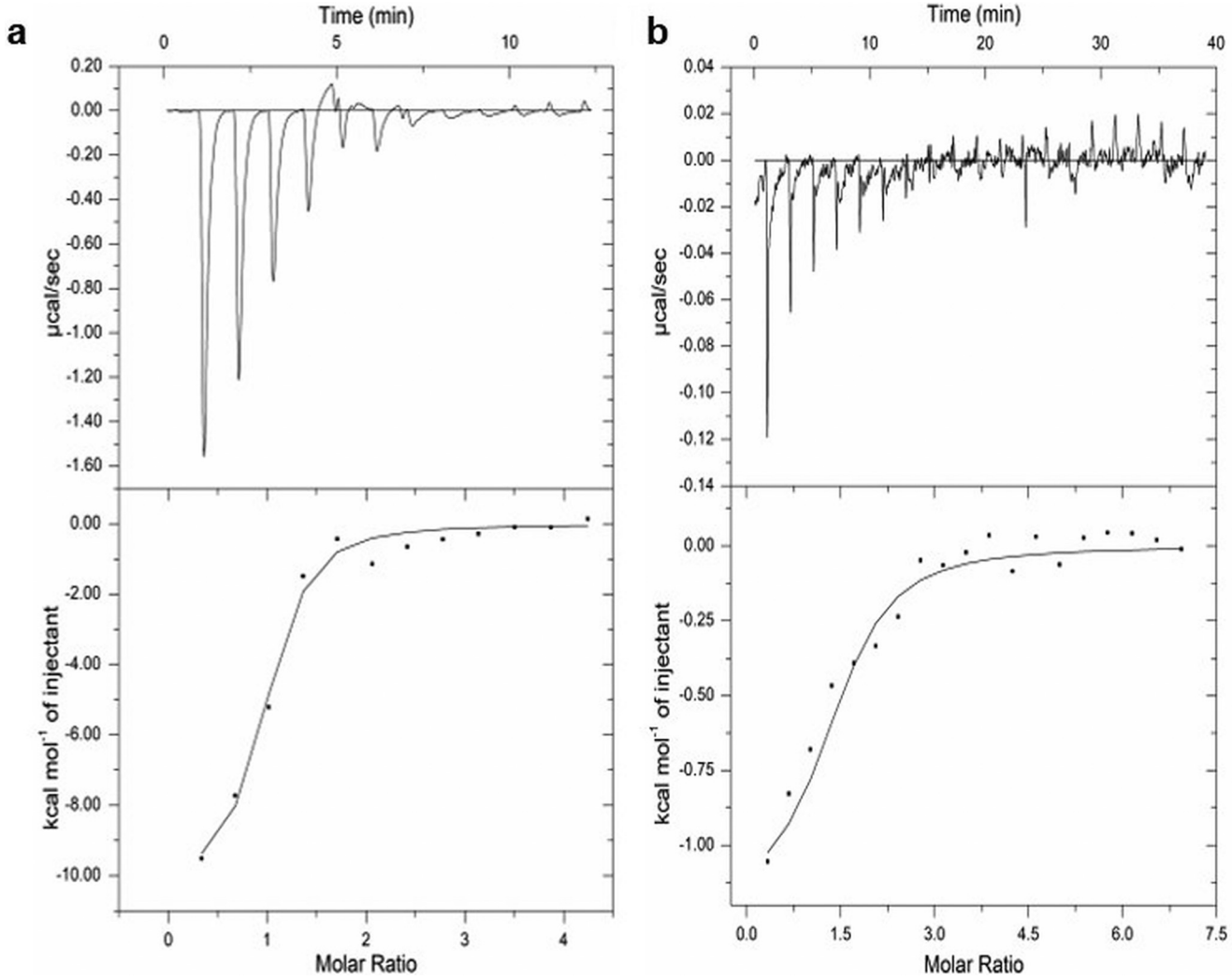

Figure 4. Binding of adenine nucleotides to Hsp90 –KU-32 complexes. *a*, 30 μM recombinant human Hsp90β was preincubated with 30 μM KU-32 and titrated against 1 mM ADP. The heat of binding was calculated after subtracting the heat of dilution from control experiments where 1 mM ADP was titrated against reaction buffer containing only KU-32. *b*, 30 μM recombinant human Hsp90β was preincubated first with 30 μM KU-32 followed by 30 μM ADP and titrated against 1 mM ATP. The heat of binding was calculated after subtracting the heat of dilution from control experiments where 1 mM ATP was titrated against reaction buffer containing only KU-32 and ADP.

32–ATP complex (Fig. S9), however, revealed an initial movement of the Hsp90 monomers toward each other (Fig. 5*a*). The RMSD between the NTDs of each monomer decreased from 135 to 85 Å (Fig. S10). This movement was restricted after ~220 ns of simulation, when Hsp90 was somewhere between its fully extended and fully closed states. During the rest of the simulation, the NTD reoriented itself with respect to the MD to attain an alternate conformation. In this intermediate state, the ATP-bound region of the NTD was found to be proximal to Arg^{392} of the MD (Fig. 5*c*), which initiates the formation of the catalytic center comprising Arg^{41}, Glu^{42}, Asn^{46}, and Arg^{392} (31). However, the ATP lid comprising residues Ala^{106}–Gly^{130} shows no movement, and its conformation is unconstrained, just as in the apo-form of Hsp90 (32). KU-32 formed strong hydrogen bonds with Ser^{532} and Ser^{586}, a strong π stacking interaction between its coumarin ring and His^{632}, and weak π stacking interactions with Pro^{588} and Pro^{533}. Thr^{537} and Lys^{538} participated in strong hydrogen bonds with the 4′-hydroxyl group of the sugar ring in KU-32 (Fig. 5*b*). Analysis of the simulation trajectory shows that KU-32 exerts its effect by bringing the two β-sheets comprising residues 525–539 in proximity to the loop comprising residues 582–590. This effect can be observed by plotting the distance between Ser^{532} (central residue in the β-sheets) and Ser^{586} (central residue in the loop) (Fig. S11*a*). The amide bond in KU-32 serves as a bridge to bring the serine residues closer (Fig. 5*b*). The average RMSD decreases from 12 to 10 Å after the first 150 ns of simulation, followed by a further decrease to 7 Å at 220 ns, after which it was stable. This movement pulls the rest of the MD closer to the CTD, which can be visualized by plotting the distance between Ser^{586} and other residues within the MD (*e.g.* Ser^{445}, located near the end of the MD, and Lys^{406}, located in the center of the MD) (Fig. S11*b*). A sharp decrease at 220 ns followed by a stable RMSD for both pairs indicated that the MD residues are now proximal to the CTD residues, resulting in a relatively compact Hsp90 structure. The RMSD was found to decrease by ~3 Å for both pairs of residues (Ser^{586}/Lys^{406} and Ser^{586}/Ser^{445}). Thus, there are large (~5 Å) local conformational changes that occur within the CTD. The rela-

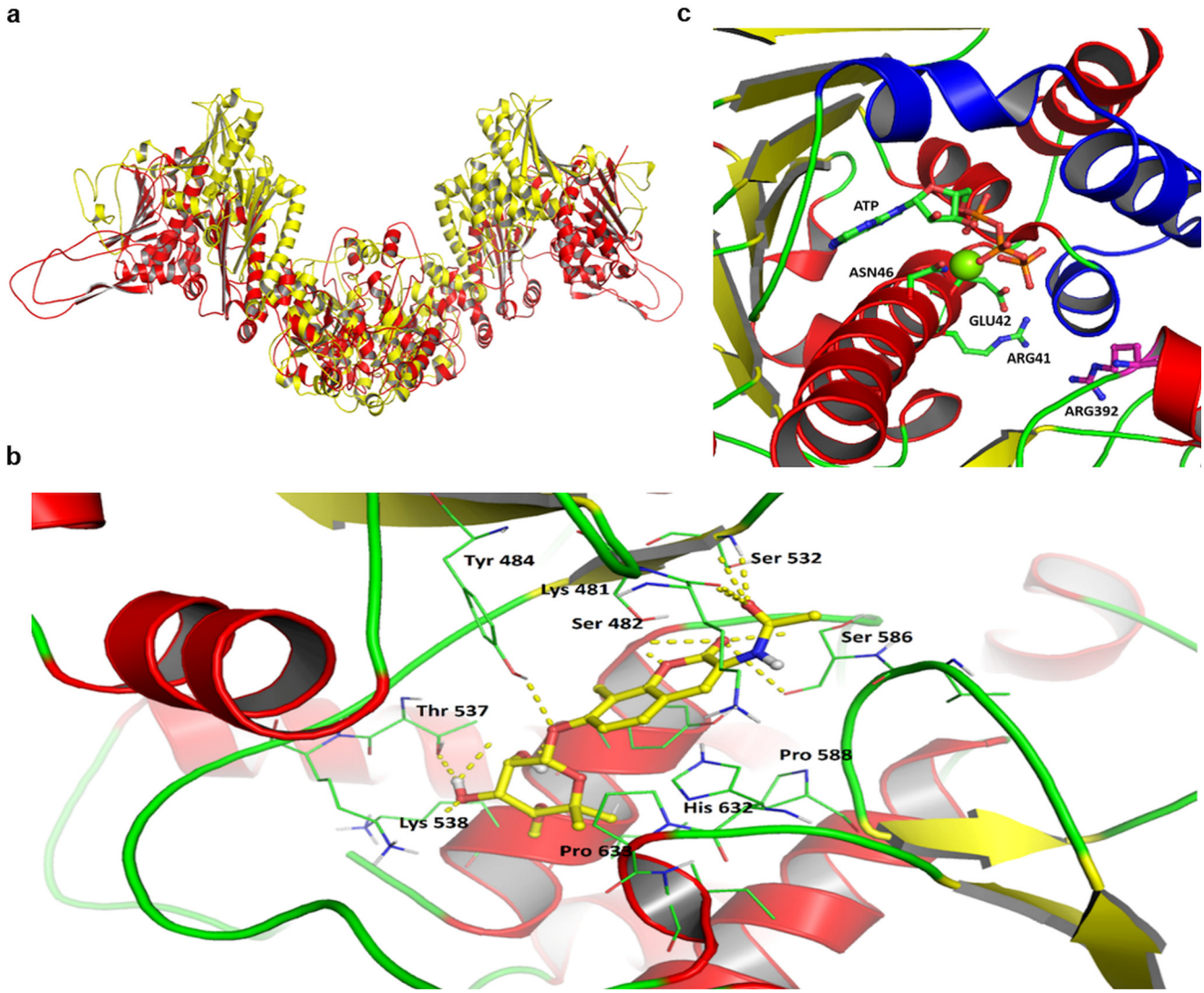

Figure 5. Conformational analysis of the simulated Hsp90–KU-32 and Hsp90–KU-32–ATP complexes. *a*, a snapshot from MD of the closing of Hsp90β upon binding of KU-32 after 420 ns. *Red* and *yellow structures* indicate conformation of Hsp90 at $t = 0$ ns and $t = 420$ ns, respectively. *b*, interaction diagram of KU-32 with Hsp90 obtained from the last snapshot of the MD trajectory. KU-32 is represented in *yellow*. Hydrogen bonds are depicted as *dotted yellow lines*. *c*, a snapshot of the ATP-Mg^{2+}–bound NTD in proximity to Arg^{392} (depicted in *pink*) obtained after 340 ns of simulating the Hsp90–KU-32–ATP complex. The ATP lid is depicted in *blue*, and the Mg^{2+} ion is depicted as a *green ball*.

tively smaller, but significant, deviations between the MD and CTD residues indicate the transfer of conformational changes to the MD. There was negligible internal conformational change in the MD, as indicated by a low RMSD value of 3.4 Å throughout the trajectory (data not shown). These changes are then relayed to the NTD, as observed by plotting the distance between the center of masses of the NTD and the MD (Fig. S12). After 220 ns, the global RMSD profile showed a gradual decrease, and at 340 ns, it showed a sudden decrease of ~4 Å, after which the RMSD was negligible. This movement implied that the NTD was stable with respect to the position of the MD. No additional structural changes were observed upon simulating the Hsp90–KU-32 complex without ATP.

Ser^{532} and Ser^{586} are critical for KU-32 binding

The structures of KU-32 and NB were analyzed to understand the divergent conformational changes undergone by Hsp90 when bound to either of them. Docking of NB at the KU-32–binding site showed the benzene ring in NB to sterically clash with the neighboring residues, making it impossible for NB to attain KU-32's conformation (Fig. S13). Further, the amide bond in NB could not bridge the critical bond between Ser^{532} and Ser^{586} (as opposed to KU-32), forcing Hsp90 to remain in its open, extended conformation. To confirm the significance of bridging the hydrogen bond between Ser^{532} and Ser^{586}, Hsp90 was mutated to substitute these two residues with alanine. The binding conformation of KU-32 docked to mutant (S532A/S586A) Hsp90 was not significantly different as compared with the modeled WT Hsp90β (Fig. S14). However, unlike the behavior of WT Hsp90 bound to KU-32, partial closing of the monomer arms was not observed during the span of the simulation with mutated (S532A/S586A) Hsp90β. The monomer arms remained in an open, extended state similar to the conformation adopted by Hsp90 when bound to NB. *In silico* studies have certain limitations and only depict a partial picture of interactions between two systems under certain

Table 6

EC_{50} values of NTD inhibitor GA and CTD binding compounds NB and KU-32 acting individually and in combination

C1, C2, and C3 represent combinations involving constant ratios of (EC_{50}) GA/(EC_{50}) NB at 1, 1:3, and 3 respectively. C4, C5, and C6 represent combinations involving varying concentrations of GA with concentrations of KU-32 fixed at 1, 10, and 100 μM, respectively. *Unpaired two-tailed *t*-tests to evaluate significant differences between EC_{50} values of compounds acting alone and in combination yielded *p* values < 0.01 in all cases except *a* and *b*, which showed no significance ($p = 0.284$) and marginal significance ($p = 0.019$), respectively.

		GA	NB	KU-32	GA + NB*			KU-32 + GA*		
					C1	C2	C3	C4	C5	C6
EC_{50}	GA	8.04	-	-	3.55	1.96	7.67[a]	35.70	43.46	48.05
	NB	-	200.46	-	66.57	110.36[b]	47.99	-	-	-
	KU-32	-	-	> 900	-	-	-	-	-	-

assumed conditions. Therefore, *in vitro* experiments were performed to determine whether the S532A/S586A mutation affected the binding of KU-32 to Hsp90. Isothermal titration calorimetry revealed that KU-32 was not able to bind the S532A/S586A mutant (Fig. S15). This indicates that Ser^{532} and Ser^{586} are critical for KU-32 binding.

Hsp90 inhibitors reduce cell viability, whereas KU-32 exhibits a cytoprotective role

From the biochemical studies performed, we observed a trend where GA and NB complemented each other's inhibition, whereas KU-32 antagonized GA-mediated inhibition of chaperone function. Cytotoxicity studies were conducted on a HeLa cell line to quantify the degree of synergy or antagonism between the pairs by computing the dose reduction index (DRI) and the combination index (CI) using CalcuSyn. DRI measures the -fold reduction in the required dose of a compound administered in a combination that will manifest activity equivalent to that elicited by the compound administered alone. CI measures the extent of synergy or antagonism between the compounds used in combination. $CI < 1$ signifies synergy, $CI = 1$ indicates additive effect, and $CI > 1$ indicates antagonism. Initially, EC_{50} values for the individual compounds were determined (Fig. S16 and Table 6). GA and NB were toxic to HeLa cells, whereas KU-32 did not significantly affect cell viability under the range of concentrations tested ($EC_{50} > 0.9$ mM). 3D plots were generated for all of the constant ratio combinations (C1–C3) involving GA and NB (Fig. S17, *a–c*). C1 displayed ~56 and 67% reduction in the EC_{50} value of GA and NB, respectively. C2 displayed a 76% reduction in the EC_{50} value of GA, and C3 displayed a 76% reduction in the EC_{50} value of NB (Table 6). The highest DRI values for GA (13.8, 4.9, and 2.9) were obtained with combinations $C3_5$, $C2_1$, and $C1_1$, respectively. The highest DRI values for NB (5.8, 3.9, and 2.3) were obtained with combinations $C3_5$, $C1_1$, and $C2_1$, respectively. The CI values obtained for these combinations were correlated with the fraction of cells (f_a) affected by the compound(s). This correlation was essential to determine the combination that was most effective at killing cancer cells. $C1_1$ ($CI = 0.61$) and $C2_1$ ($CI = 0.64$) showed moderate synergy at values of $f_a \leq 0.6$, whereas $C3_5$ ($CI = 0.25$) showed extremely high synergy at values of $f_a > 0.8$ as depicted by the f_a–CI plot (Fig. 6). Thus, $C3_5$ was found to be the most effective synergistic combination not only in terms of reducing cell viability, but also in producing the highest reduction with respect to the effective doses of GA and NB in combination. Nonconstant ratio combinations involving GA and KU-32 were formed by varying the concentration of GA while keeping the concentration of KU-32 fixed at 1 μM (C4), 10 μM (C5), and 100 μM (C6). EC_{50} values of GA were found to increase by 4.5, 5.4, and 6 times in parent combinations C4, C5, and C6, respectively, as compared with control experiments that included GA alone (Table 6). In the case of GA, the lowest DRI values of 0.32, 0.23, and 0.19 were obtained in the case of combinations $C4_5$, $C5_6$, and $C6_6$, respectively. $C4_5$ ($CI = 2.27$) was found to exhibit moderate antagonism, whereas $C5_6$ ($CI = 4.38$) and $C6_6$ ($CI = 5.38$) were found to exhibit a greater degree of antagonism at f_a values of 0.53, 0.54, and 0.48, respectively (Fig. 6). This indicated a positive correlation between the dose-dependent enhancement of cell viability (Fig. S17*d*) and the degree of antagonism exhibited by these combinations. Taken together, these observations suggest that KU-32 acts as an antagonist to GA-mediated cytotoxicity by effectively increasing both cell viability and the GA concentration required to elicit the same cytotoxic effect elicited by GA alone.

NB and GA prevent luciferase renaturation, whereas KU-32 acts as a stimulator

To understand how Hsp90 binders affect luciferase renaturation and to determine whether the changes in cell viability observed in their presence were a result of either inactivation or renaturation of substrate proteins, heat shock studies were carried out on HeLa cells expressing firefly luciferase. Luciferase activity decreased by ~98% upon placing the cells at 50 °C for about ~6 min, without significant loss in cell viability. Upon incubation at 37 °C, luciferase renaturation occurred in a time-dependent fashion, with cells incubated for 3 h post heat shock exhibiting ~50% recovery (Fig. S18). HeLa cells were incubated with varying concentrations of GA, NB, and KU-32 after being subjected to heat shock. Luciferase activity was measured 3 h post-heat shock. Cells incubated with GA and NB showed a gradual reduction in luciferase activity, with the highest reduction of ~70 and 65% obtained at 5 μM GA (Fig. 7*a*) and 100 μM NB (represented by *filled circles* in Fig. 7*b*), respectively. Conversely, a gradual increase in luciferase activity was observed at lower concentrations of KU-32. Saturation was attained at concentrations of 25–50 μM KU-32, which manifested a ~2.5 times increase in luciferase luminescence relative to the control experiments (represented by *filled circles* in Fig. 7*c*). The EC_{50} values of GA, NB, and KU-32 were calculated to be 0.34 ± 0.02, 17.96 ± 4.07, and 5.71 ± 0.59 μM, respectively.

NB acts as an agonist, whereas KU-32 antagonizes GA-mediated inhibition of luciferase renaturation

To determine how NB and KU-32 affect the renaturation of luciferase in the presence of GA, combination studies were conducted using 5 μM GA and varying concentrations of either NB or KU-32. Luciferase renaturation was partially hindered in combinations involving GA and KU-32 as compared with KU-32 acting alone, and no significant change was observed as compared with the control experiments (represented by *filled*

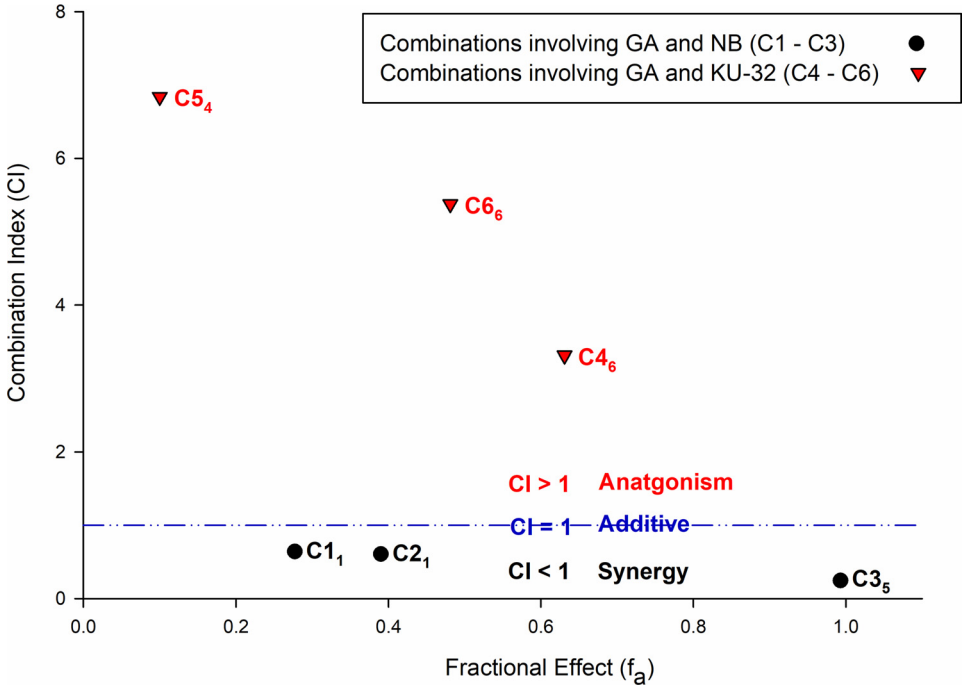

Figure 6. f_a–CI plot. CI values for the best performing pairs within a parent combination were plotted against their respective f_a values. C1, C2, and C3 represent constant-ratio parent combinations (each consisting of five pairs) formed by keeping the ratio of (EC_{50}) GA/(EC_{50}) NB at 1, 1/3, and 3, respectively. C4, C5, and C6 represent nonconstant ratio parent combinations (each consisting of six pairs) formed by varying the concentration of GA while keeping the concentration of KU-32 fixed at 1, 10, and 100 μM, respectively.

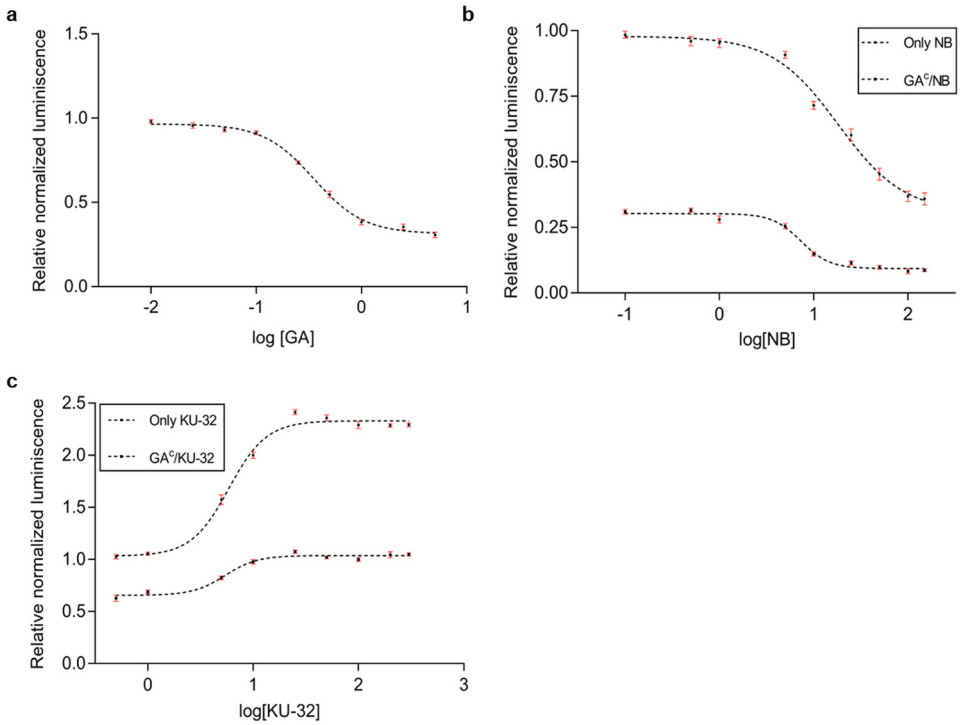

Figure 7. Renaturation of luciferase in the presence of Hsp90 NTD and CTD binders acting alone and in combination. Firefly luciferase activity was measured in the presence of individual compounds followed by studies that included a combination of either GA and NB or GA and KU-32. *a*, luciferase renaturation was measured in the presence of varying concentrations (0.01–5 μM) of NTD inhibitor GA. *b*, luciferase renaturation was measured in the presence of varying concentrations of CTD inhibitor NB (0.1–150 μM) acting alone and when combined with 5 μM GA (as represented by *GA^C/NB*). *c*, luciferase renaturation was measured in the presence of KU-32 (0.5–300 μM) acting alone and when combined with 5 μM GA (as represented by *GA^C/KU-32*). In all experiments, luminescence was measured after cells were allowed to renature for 180 min in the presence of compounds acting either alone or in combination. The normalized luminescence values were computed relative to control experiments where renaturation of luciferase was measured in the absence of compound(s). *Error bars*, S.D.

squares in Fig. 7*c*). The EC_{50} of GA in this combination was calculated to be 5.4 ± 0.73 μM. This is significantly higher than the value obtained for GA alone and demonstrates the antagonistic behavior of KU-32 with respect to GA. On the other hand, studies involving GA and NB showed increased efficacy in inhibiting luciferase renaturation (represented by *filled*

squares in Fig. 7*b*), as evidenced by a significant decrease in the EC_{50} value of NB (7.37 ± 0.78 μM). These results suggested that GA enhances the inhibitory activity of NB and that GA combined with NB exhibits a greater degree of efficacy in inhibiting Hsp90 chaperone function.

Discussion

Hsp90's chaperone function depends upon the ATP hydrolysis cycle that facilitates folding of nascent polypeptides, rendering them biologically active. Although most of the NTD inhibitors have been well-characterized with respect to their inhibition of ATP binding to the NTD of Hsp90, limited information is available about the mechanism of action of CTD inhibitors. Our interest in KU-32 was generated because of studies (21, 25) that indicated that KU-32 was behaving differently than any of the known inhibitors, including its parent compound NB. It was hypothesized that detailed investigation into its mode of action would reveal interesting features about the molecule's ability to alter the structure and, hence, the function of the chaperone. Differences in the structural changes induced by the binding of KU-32 and NB to Hsp90 could lead to a better understanding of the divergent evolution of these synthetic compounds. A real-time ATP-regenerating assay was carried out to understand the role of NTD and CTD binders in modulating Hsp90's ATPase cycle. We observed that GA and NB reduced the ATPase activity in a dose-dependent and dose-independent fashion, respectively, whereas KU-32 manifested a significant increase in ATP hydrolysis. To determine whether the KU-32–mediated stimulation of ATPase activity was hindered in the presence of GA, we designed studies that involved a combination of GA and either of the CTD binders, NB or KU-32. When GA and NB were combined, they manifested a significantly greater decrease in the Hsp90 ATPase activity relative to GA or NB alone. Interestingly, GA did not alter the ATPase activity of the chaperone when it was co-administered with KU-32. These data suggested that KU-32 nullifies the GA-mediated inhibition of Hsp90's ATPase function.

This initial study prompted a more detailed analysis of how these ligands affect ATP binding and whether they allosterically regulate the binding of one another. For this purpose, isothermal titration calorimetry studies were conducted where ATP was titrated against Hsp90 bound to either NTD or CTD binders. Not surprisingly, ATP was unable to bind Hsp90 prebound to GA or NB. This is because GA is a competitive inhibitor of ATP and has a higher binding affinity, whereas NB bound to the Hsp90 CTD allosterically inhibits ATP binding to the NTD. This supports the previously reported negative allosteric regulation of the Hsp90 NTD by the CTD (15, 18). However, KU-32 did not hinder ATP binding to Hsp90. Furthermore, ATP binding was abrogated when Hsp90 was bound to both GA and NB, whereas it bound the Hsp90–GA–KU-32 complex with similar affinity as compared with the Hsp90–KU-32 complex and Hsp90 alone. To further validate the allosteric cross-talk mediated by the CTD and the NTD binders, GA binding to Hsp90–NB and Hsp90–KU-32 complexes and NB and KU-32 binding to the Hsp90–GA complex were investigated. Both NB and KU-32 negatively regulated GA binding to the NTD, with KU-32 exhibiting a greater degree of regulation. These observations suggested that the Hsp90–KU-32 complex acquires an intermediate conformation that preferentially binds ATP but not GA. This explains why we observed similar Hsp90 ATPase activity when KU-32 was combined with GA as compared with KU-32 acting alone. ATP cannot displace GA bound to the extended, apo-state of Hsp90 but was observed to bind to this intermediate state induced by KU-32 binding. This suggested that the induced conformation does not resemble the apo-state of Hsp90. Moreover, this unique conformation induced by KU-32 binding is not consistent with the closed "tensed" state of Hsp90, as little chance of ATP binding can occur upon achievement of this state. Thus, we concluded that this conformation lay somewhere between the open and the closed states of the chaperone, and KU-32 binding to the CTD positively regulates ATP binding to the NTD in an allosteric manner. Conversely, the Hsp90–GA complex was able to bind both KU-32 and NB; however, their binding affinities were reduced (10–20 times). This suggested negative allosteric cross-talk in a bidirectional manner with respect to the Hsp90 binders with the negative allosteric regulation of the NTD by the CTD binders being relatively stronger. Why did we observe only a slight reduction in Hsp90 ATPase activity in combinations involving GA and NB when the binding affinity of GA was found to be drastically reduced to the Hsp90–NB complex and vice versa? This can be explained as follows: the binding affinity of GA is far greater than that of ATP to the Hsp90–NB complex. One could argue that the difference in concentration of ATP and GA in the ATPase assay was ~80 times, whereas the difference in their respective binding affinities to the Hsp90–NB complex was ~100 times. Hence, the event of GA binding to this complex was slightly more probable than that of ATP binding.

We were interested to determine whether KU-32 additionally affected the ADP-bound conformation of Hsp90 and whether it could promote ADP release by mitigating ADP binding to Hsp90. Because ADP has a higher binding affinity to Hsp90 than ATP and their binding sites overlap, Hsp90 cannot bind ATP if it is already bound to ADP. Therefore, the indirect release of ADP by monitoring the binding of ATP to the Hsp90–KU-32–ADP complex was investigated. Indeed, ATP was observed to bind the complex with a higher affinity as compared with free Hsp90, suggesting that KU-32 induced ADP release and allowed ATP binding, thus preparing Hsp90 for another round of ATP hydrolysis. This finding is significant in the context of the ATPase cycle, as there could be multiple stages at which KU-32 modulates Hsp90 function. However, the conformation of the ADP-bound apo-state of Hsp90 (obtained in this study) could be different from the kinetic ADP-bound intermediate in the ATPase cycle.

Studies have shown that two different classes of compounds having different mechanisms of action could act in a synergistic manner (33). We wanted to investigate whether a synergistic combination of GA and NB existed that would further attenuate the viability of cancerous cells. We also wanted to determine whether KU-32 antagonized GA-induced cytotoxicity as was observed in our prior experiments. Cells incubated with KU-32 showed negligible loss in viability. Conversely, GA and NB were found to be cytotoxic. Certain combinations like $C1_1$ and $C2_1$, warrant *in vivo* testing, as they produce high DRI values and are

moderately synergistic. Such studies could be extended to target other chaperone systems (Hsp70/Hsp40) in the treatment of cancer in conjunction with existing modes of therapy. Despite GA and NB exhibiting excellent synergy and the highest DRI value in $C3_5$, it should not be considered a potent combination, as GA at 60 μM and NB at 375 μM (7.5 and 2.5 times their respective EC_{50} values) are highly toxic. Most combinations involving KU-32 and GA showed a high degree of antagonism, which reiterates the cytoprotective role played by KU-32.

Folding of nascent proteins or renaturation of partially unfolded polypeptides by Hsp90 depends on its ATPase activity. Our *in vitro* results show that Hsp90 binders affect its ATPase activity, and hence, we expected them to modulate the renaturation of denatured luciferase by endogenous Hsp90. Keeping in line with our prior results, GA and NB acted as inhibitors, whereas KU-32 enhanced Hsp90's ability to renature luciferase. Combinatorial studies involving GA and NB manifested enhanced inhibition as compared with either NB or GA, but when coupled with KU-32, GA's inhibition was ablated.

In silico studies with the modeled hHsp90β dimer provided insights into the local and global conformational changes manifested by KU-32 on the structure of the Hsp90 dimer, which might provide clues regarding the stimulation of Hsp90's function when bound to KU-32. It was observed that KU-32 acts to bring the monomer arms of Hsp90 in proximity, thereby disposing them to a more compact, closed state that eventually leads to ATP hydrolysis. Our MD simulations of the Hsp90–KU-32–ATP complex have indicated formation of the catalytic center that facilitates ATP hydrolysis by bringing Arg^{392} in proximity to the NTD of each monomer. However, it is not yet an active ATP-bound conformation but rather an inactive "potentiated" ATP bound state that, upon structural transitions of the ATP lid and the NTD loop, could reach its active state (31, 32). The distance between the Hsp90 monomers after 420 ns of simulation is not small enough to allow interdomain interactions. Interdomain interactions do not play a role in inducing ATP hydrolysis but stabilize the transient conformation that is capable of hydrolyzing ATP by reinforcing the cis interactions of each monomer and stabilizing the correct NTD-MD conformation (34, 35). Thus, the intermediate conformation of Hsp90 induced by KU-32 is not stable or entropically constrained enough to induce ATP hydrolysis. The active "ready-to-hydrolyze ATP" state is extremely difficult to attain in a classical MD simulation and may require quantum simulations to reach the millisecond time scale, where such transitions could be observed, as shown by Zhang *et al.* (36). This intermediate was also unable to bind GA as inferred from our ATPase assay. This inability to bind may result from the relatively large Van der Waal's volume for GA (523 $Å^3$) as compared with ATP (341 $Å^3$). Such a large volume may result in steric hindrance and force GA to be less likely to access the binding site in the KU-32–induced conformation.

We hypothesize that the "partially closed" intermediate (I_i) observed in our MD studies enabled Hsp90 to hydrolyze ATP at a faster rate. This might be explained by considering that Hsp90, when bound to KU-32, switches between this intermediate conformation (transition to this state from the apo-state occurs in the nanosecond time scale in our MD simulation) and the "closed" state, instead of undergoing transition from the apo-state to the closed state, thereby reducing the time taken to switch to the closed state.

We have summarized the mode of action of NB and its synthetic analogue KU-32 as shown in Fig. 8 (*a* and *b*). NB allosterically inhibited Hsp90 chaperone functions, whereas KU-32 was found to stimulate them. This stimulation of Hsp90 chaperone activity by KU-32 is a relatively novel finding and brings about a new paradigm in the understanding of the role of CTD binders in regulating Hsp90 function as well as in the design of new compounds that stimulate Hsp90's function within the cell. The reason for this divergent behavior lies in the observation that KU-32 lacks the 4-hydroxyl coumarin moiety of NB (37) that led to steric clashes when NB was docked at the KU-32– binding site. Additionally, unlike KU-32, the amide bond in NB was not able to mediate the hydrogen bond between Ser^{532} and Ser^{586} of the CTD. Our *in vitro* experiments with the Hsp90 mutant confirm that these two residues are critical for KU-32 binding. They act as a starting point for the cascade of conformational changes observed across the length of the protein. However, our simulations of the mutant Hsp90–KU-32 complex showed that KU-32 bound stably to the mutant Hsp90 and did not dissociate from the CTD. The contradictory results may be the consequence of utilizing different time scales; the length of our simulations lay in the nanosecond time scale, whereas the stable binding (or no binding) event monitored through ITC lay in the millisecond time scale. Hence, it is entirely possible that upon extending the length of the simulation, one could observe the dissociation of KU-32 from its binding cavity in the mutant Hsp90.

Hsp90 plays a key role in protein quality control by maintaining a balance between polypeptides that can be folded or refolded and aggregates or misfolded intermediates that must be degraded to prevent cell death (38–40). Neuropathies or neurodegenerative disorders are generally caused by accumulation of misfolded proteins or toxic aggregates inside the cell that result when this balance is altered, and the chaperone machinery is unable to cope with the copious amount of toxic aggregates (33, 34). Recently, a KU-32 analogue (41) has entered Phase II trials for treating neuropathies (trial data are confidential). We believe that KU-32 and its analogue stimulate the chaperone function of Hsp90 and most likely reduce the load of misfolded proteins inside the cell. This can happen either through enhancing Hsp90's folding ability or through enhancing Hsp90's binding with misfolded substrate proteins (reducing their local concentration, which may lower their tendency to form aggregates). However, further experiments will be required to pinpoint the mechanism of action.

Experimental procedures

Chemicals and reagents

PCR reagents were obtained from Thermo Scientific. DpnI restriction enzyme was obtained from Agilent (catalog no. 200519-53). Primers for PCR amplification were synthesized from Integrated DNA Technologies. Novobiocin (catalog no. 18457) and geldanamycin (catalog no. 13355) were purchased

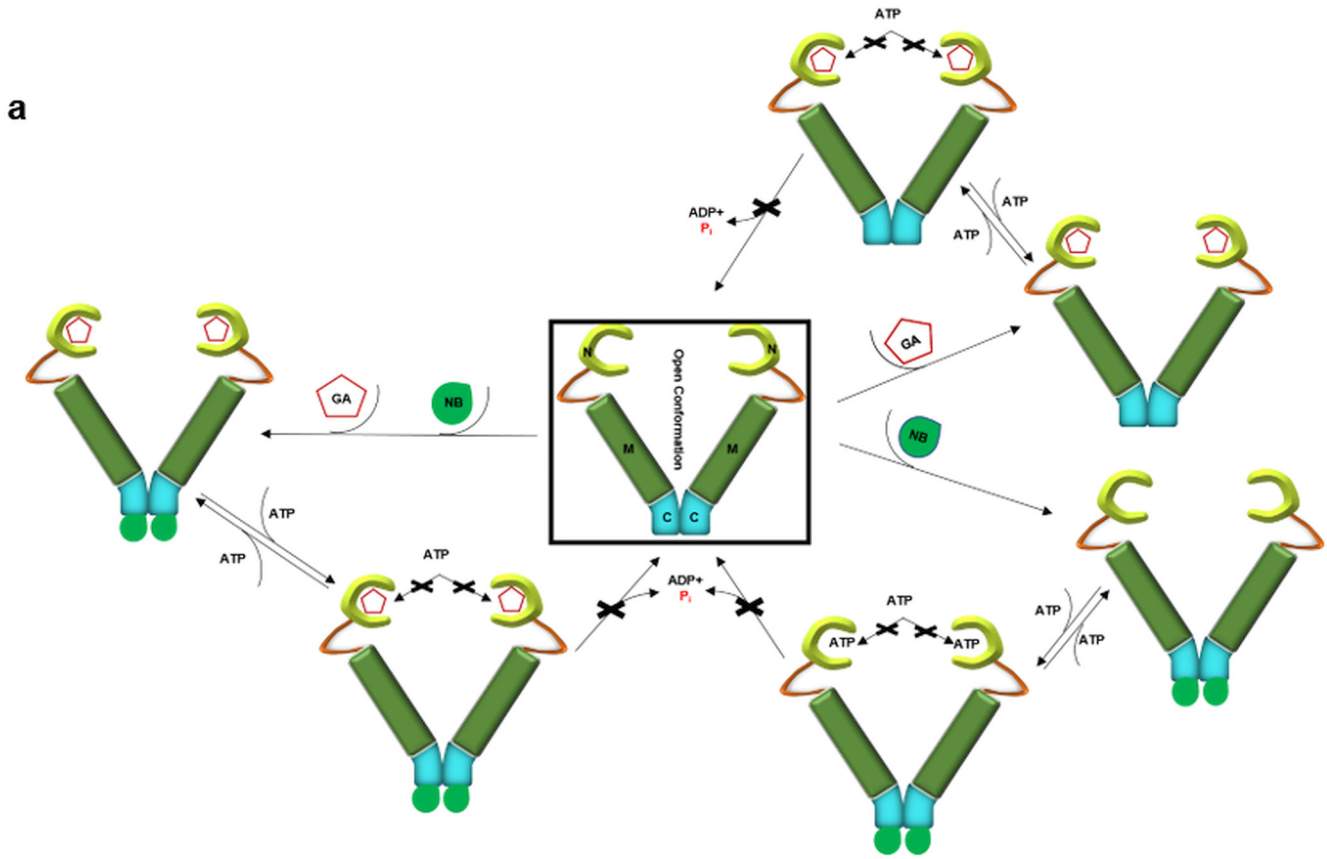
a
ATP
ADP+
P_i
ATP
ATP
GA
NB
N
N
Open Conformation
M
M
C
C
GA
NB
ATP
ATP
ATP
ADP+
P_i
ATP
ATP
ATP
ATP
ATP

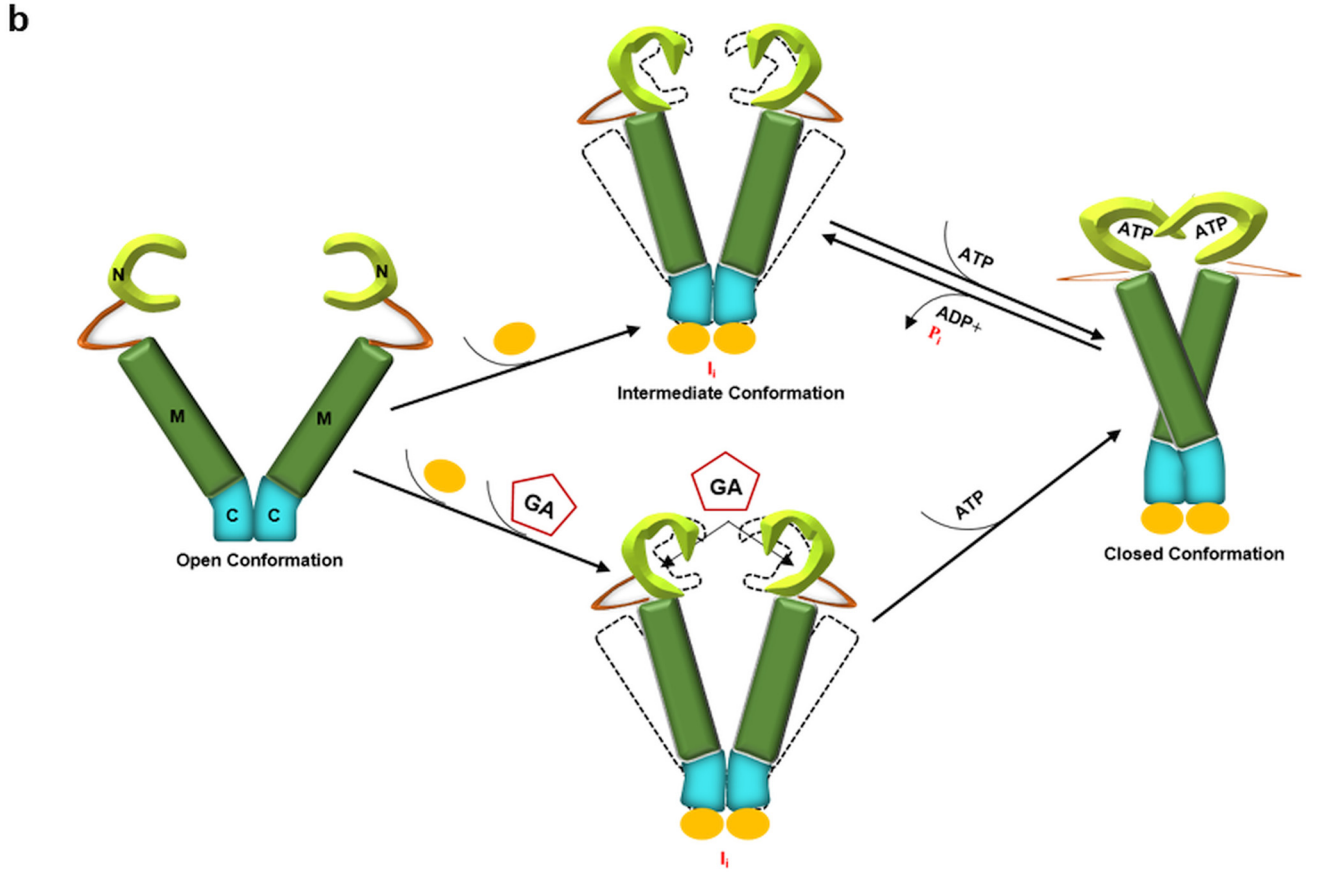
b
N
N
M
M
C
C
Open Conformation
I_i
Intermediate Conformation
ATP
ADP+
P_i
ATP
ATP
GA
GA
ATP
I_i
Closed Conformation

from Cayman Chemicals. KU-32 was a kind gift from Dr. Brian Blagg. Cell transfection reagent Polyfect was purchased from Qiagen (New Delhi, India) (catalog no. 301105). The Dual-Luciferase assay kit was purchased from Promega (catalog no. E1910). Components of the ATP-regenerating system, namely the pyruvate kinase/lactate dehydrogenase enzyme system in 50% glycerol (catalog no. P0294), NADH disodium salt hydrate (catalog no. 43420), ATP disodium salt (catalog no. A26209), and phosphoenolpyruvate monopotassium salt (catalog no. P1727), were all purchased from Sigma (Bangalore, India). Cell culture medium components were from GIBCO (Bangalore, India). 3-(4,5-Dimethylthiazol-2-yl)-2,5-diphenyltetrazolium bromide (MTT) reagent was purchased from Sisco Research Laboratories Pvt. Ltd. (catalog no. 33611). All other chemicals were obtained from HiMedia/Merck Millipore (Mumbai, India).

Drug stocks and combinations

ATPase assay—GA, NB, and KU-32 were dissolved in DMSO to obtain stock concentrations of 9, 100, and 50 mM, respectively. Final concentrations used in the ATPase assay for individual drugs ranged from 6 to 90 μM. For combinatorial studies, 6 μM GA and 90 μM NB were used either as a mixture (combined and preincubated with Hsp90) or as a sequential addition of GA or NB first followed by an incubation period of 4–5 min and the addition of the other drug. A similar protocol was used for GA (6 μM) and KU-32 (90 μM) in combinatorial studies.

In vitro cytotoxic studies—For single drug studies, GA concentration ranged from 50 nM to 90 μM, NB concentration ranged from 500 nM to 800 μM, and KU-32 concentration ranged from 50 nM to 200 μM. In the cytotoxicity assays involving single drugs, at least seven data points were used to calculate the EC_{50} values. EC_{50} values of GA and NB were initially determined from cytotoxic studies, and three different ratios of EC_{50} values were used for combinatorial studies (EC_{50} GA/EC_{50} NB = 1, 3, and 0.34). Table S3 (*a* and *b*) lists the combinations used for cytotoxicity evaluations for combinatorial studies involving GA plus NB and GA plus KU-32, respectively.

Heat shock experiment—For individual drug studies, GA concentrations used ranged from 0.01 to 5 μM; KU-32 concentrations used ranged from 0.5 to 300 μM, and NB concentrations used ranged from 0.1 to 150 μM. Table S4 shows the concentration of each compound used in the combinatorial studies involving either GA plus NB or GA plus KU-32.

Site-directed mutagenesis

Site-directed mutagenesis was performed to mutate Ser^{532} and Ser^{586} of WT Hsp90 to alanine. To create the S532A/S586A mutant, two sets of primers were designed. The forward and reverse primers designed for the S532A mutation were 5′-GGAATTTGATGGGAAGGCCCTGGTCTCAGTTACC-3′ and 5′-GGTAACTGAGACCAGGGCCTTCCCATCAAATTCC-3′, respectively. The forward and reverse primers designed for the S586A mutation were 5′-CCAATAGACTTGTGGCTTCACCTTGCTGCATTG-3′ and 5′-CAATGCAGCAAGGTGAAGCCACAAGTCTATTGG-3′, respectively. The PCR amplification conditions include the following steps: initial denaturation at 95 °C (3 min), denaturation at 95 °C (30 s), annealing at 57 °C (45 s) for S532A and at 60 °C (45 s) for S586A, extension at 72 °C (8 min), and a final extension at 72 °C (15 min). The total number of PCR cycles was 18. The amplified plasmid(s) was then treated with DpnI restriction enzyme (Agilent) for 30 min at 37 °C to remove methylated parental DNA, followed by deactivation of the enzyme at 65 °C for 20 min. The amplification was confirmed on a 1% agarose gel. DpnI-treated PCR-amplified product was subsequently transformed into competent DH5α cells. The plasmid was isolated from the transformed colonies, and the mutations were confirmed by DNA sequencing.

Expression and purification

Full-length recombinant human His-tagged Hsp90β cloned in pET-28a was kindly gifted by Dr. Johannes Buchner. It was transformed in *Escherichia coli* BL21(DE3) competent cells and purified as reported previously (34). Briefly, transformed cells at an OD of 0.8–1 were induced at 37 °C for 4 h by adding 1 mM isopropyl β-D-1-thiogalactopyranoside. Cells were lysed in buffer containing 50 mM sodium phosphate, 500 mM NaCl, 0.2 mM EDTA, 1 mM phenylmethylsulfonyl fluoride, and 1 mg/ml lysozyme. The supernatant obtained after sonication was loaded onto a nickel-nitrilotriacetic acid column, and the protein was eluted at 150–200 mM imidazole. This was followed by dialysis in buffer containing 20 mM Tris-HCl and 20 mM NaCl, and the dialysate was loaded onto a Q-Sepharose column for anion-exchange chromatography. The protein was eluted at 400 mM NaCl using a linear gradient. Finally, anion-exchange chromatography fractions were pooled and loaded onto a Superdex 200 column for gel filtration chromatography. The pure protein thus obtained was filtered using a 0.22-μm syringe filter and stored in buffer containing 40 mM HEPES and 300 mM KCl. The purity of the eluted protein was checked by SDS-PAGE. The concentration of the pure protein was determined spectrophotometrically by the Beer–Lambert law, using the molar extinction coefficient of Hsp90β (57,760 M^{-1} cm^{-1}). The S532A/S586A mutant was purified using the same protocol.

ATPase assay

The ATPase assay was performed using the ATP regeneration system as described previously (42). Concentrations of recombinant human Hsp90β were kept at 6 μM throughout the

Figure 8. *Schematic representation* of the proposed mechanism of action of Hsp90 NTD and CTD binders acting alone and in combination. *a*, GA and NB inhibit ATP binding to the NTD of Hsp90 and prevent ATP hydrolysis by keeping Hsp90 in its open state. When GA and NB are combined, they complement each other in further inhibiting ATP binding to Hsp90 and its subsequent hydrolysis. For the sake of clarity, only one of the three studied conditions of the combination has been depicted. *b*, binding of KU-32 to the open "apo" Hsp90 state induces inter- and intradomain conformational change resulting in the formation of an intermediate (I_i) state. Upon ATP binding, Hsp90 attains its closed "committed to ATP hydrolysis" conformation. Following ATP hydrolysis and the release of ADP and P_i, Hsp90 returns to I_i instead of its apo-state, which probably explains the relatively faster rates of ATP hydrolysis in the presence of KU-32. GA, unlike ATP, is unable to bind this intermediate conformation (when GA and KU-32 are combined) and hence cannot inhibit ATP hydrolysis. The KU-32 molecule is represented as a *yellow circle*.

experiments. For all compound studies (see "Drug stocks and combinations"), Hsp90 was preincubated with a single or a combination of compounds before being added to the reaction mixture. Assays were measured in a buffer (pH 7.5) containing 50 mM HEPES, 20 mM KCl, 10 mM $MgCl_2$, 0.5 mM ATP, 0.15 mM NADH, PK/LDH (1/150 of the reaction volume), and 0.7 mM PEP at 37 °C. Control experiments performed to negate UV-induced NADH degradation did not include ATP in the reaction mixture. The time interval between two consecutive readings was 3 min. The decrease in NADH absorbance at 340 nm was monitored by a microplate reader (Thermo Scientific Multi-Skan Go). Data were recorded for 60 min and were evaluated using the SigmaPlot software package. The raw NADH plot obtained was converted to a relative cumulative NADH absorbance plot through the following equation,

$$(\Delta\ \mathrm{NADH})_x = (T_0 - C_0) - (T_x - C_x) \qquad \text{(Eq. 1)}$$

where the relative cumulative absorbance for time point x is represented by $(\Delta\ \mathrm{NADH})_x$. T_0 and T_x are test samples containing compound(s) at time points 0 and x ($x \geq 0$ and $x \leq 20$), respectively. C_0 and C_x are control samples without ATP at time points 0 and x, respectively. The Hsp90 ATPase rate was calculated from the following equation,

$$\text{ATPase rate}\left(\frac{\mu\text{M ATP}}{\text{min}\cdot\mu\text{M Hsp90}}\right) = \frac{\text{Rate of } A_{340} \text{ signal loss}\left(\frac{\text{OD}}{\text{min}}\right)}{\text{pl (cm)}\cdot\text{extinction coefficient of NADH } (\mu\text{M}^{-1}\,\text{cm}^{-1})\cdot\text{Hsp90 } (\mu\text{M})} \qquad \text{(Eq. 2)}$$

where pl represents path length. The rates of A_{340} signal loss were calculated from the slopes obtained after performing global regression analysis on the fitted curves. In all cases, the linear portion of the assay data was chosen to calculate the rate of signal loss except for experiments involving KU-32, where the initial exponential rate of signal loss was considered. All assays were performed in triplicate.

Isothermal titration calorimetry

Thermodynamic parameters of ATP, ADP, and other small molecules binding to recombinant human Hsp90β were obtained using a MicroCal ITC200 microcalorimeter (GE Healthcare). The calorimeter had a reaction cell volume of 200 μl and a syringe volume of 40 μl. For all titration experiments, Hsp90 and the ligands were diluted into a buffer containing 50 mM HEPES, 20 mM KCl, and 10 mM $MgCl_2$. The heat released or absorbed due to the binding of 1 mM ATP or ADP to 30 μM Hsp90 was measured at 25 °C. The ligands were injected in a stepwise fashion into the reaction cell with an injection volume of 1.5–2.5 μl and for a duration of 4 s. The interval between injections was 60–120 s. To determine the binding affinity of various small molecules used in this study, 20 μM Hsp90 was titrated against 100 μM of GA, NB, and KU-32. Binding of KU-32 to S532A/S586A Hsp90 was investigated by titrating 100 μM KU-32 against a 20 μM concentration of this mutant protein. To check binding of ATP to Hsp90 in the presence of small molecules, 30 μM Hsp90 was incubated with 30 μM GA or NB or KU-32 and titrated against 1 mM ATP. To determine the effect of GA on the binding of NB or KU-32 to the CTD of Hsp90, 20 μM Hsp90 was incubated with 20 μM GA and titrated against a 100 μM concentration of either NB or KU-32. To evaluate the effect of CTD binders NB and KU-32 on the binding of GA, 20 μM Hsp90 was incubated with 20 μM NB or KU-32 and titrated against 100 μM GA. To determine whether NB and KU-32 bound to the same region of the CTD of Hsp90, 20 μM Hsp90 was incubated with 20 μM KU-32 and titrated against 100 μM NB. Combinatorial studies were carried out by incubating 30 μM Hsp90 with a mixture of either 30 μM GA and 30 μM KU-32 or 30 μM GA and 30 μM NB (in separate experiments), and the complexes were subsequently titrated against 1 mM ATP. ADP binding to Hsp90 in the presence of either NB or KU-32 was investigated by titrating a mixture of 30 μM Hsp90 and 30 μM NB or KU-32 against 1 mM ADP. ADP binding to the Hsp90–GA complex was investigated by titrating a mixture of 30 μM Hsp90 and 30 μM GA against 0.15 mM or 1 mM ADP. ADP release upon binding of KU-32 to Hsp90 was monitored as follows. 30 μM protein was first incubated with 30 μM of KU-32 followed by 30 μM ADP, and the mixture was titrated against 1 mM ATP. The heat released or absorbed from control experiments was subtracted from the heat measured for each of the binding reactions. The data were analyzed and fitted using Microcal Origin software provided with the instrument. The experimental data were fitted using a single class of sites (n = 1) model for binding of compound(s) to Hsp90. The enthalpy of binding (ΔH) and the Gibbs free energy (ΔG) were also determined from the heat release measurement and are independent of the binding model. The DMSO concentration inside the calorimeter cell and the syringe was kept at or below 1% (v/v).

Cell culture

HeLa cells were procured from NCCS (Pune, India). Firefly luciferase cloned in pcDNA-3 vector was kindly gifted by Dr. William Kaelin (43). The cells were maintained in Dulbecco's modified Eagle's medium containing 10% fetal bovine serum. Transient transfections in 24-well plates were carried out when the cells reached 80–90% confluence. A 250-ng aliquot of plasmid was transfected using Polyfect transfection reagent. 24 h post-transfection, cells were lysed using lysis buffer provided in the Dual-Luciferase assay kit, and the lysate was collected in 100-μl volumes. Luminescence measurements were carried out in 96-well plates using the MicroBeta scintillation unit (PerkinElmer Life Sciences). Briefly 25 μl of luciferase assay reagent was added to 5 μl of the lysate, and the luminescence was measured at 550 nm. All values were normalized with respect to control samples (only luciferase assay reagent). EC_{50} values obtained for luciferase renaturation in the presence of compounds acting individually and in combination (GA/NB or GA/KU-32) were computed using GraphPad Prism (version 6.0, GraphPad Software). The highest concentrations of GA and NB employed in these experiments were significantly lower than their respective EC_{50} values.

Heat shock experiment

HeLa cells were subjected to heat shock as described previously (21) with certain modifications. Briefly, prewarmed serum-free medium at 50 °C was added to the cells in 24-well plates, and the plates were then placed for 6 min in a water bath preheated to 50 °C. Post-heat shock, medium was discarded and replaced with either fresh serum-free medium or a mixture of compound(s) in serum-free medium (see "Drug stocks and combinations"). Cells were then incubated at 37 °C in 5% CO_2 for 3 h. Cells were taken out at different time points (before heat shock, immediately after heat shock, and after 3-h incubation), lysed, and assayed for luciferase activity. All assays were performed in quadruplicate. Final DMSO concentration was <1% (v/v) for all compounds involved in the assay.

In vitro cytotoxicity assays

To determine the effect of compounds on the viability of HeLa cells, the MTT assay was performed. Cells were trypsinized, washed twice with PBS, and plated in a 96-well plate at a seeding density of 1.5×10^4 cells/well. After attaining 80–90% confluence, the cells were treated with the compounds (see "Drug stocks and combinations") and kept at 37 °C in 5% CO_2 for 24 h. Postincubation, 100 μl of MTT (1 mg/ml in PBS) was added to each well, and cells were further incubated at 37 °C in 5% CO_2 for 3–4 h. The formazan crystals formed were then dissolved in 100 μl of DMSO, and the absorbance was measured using a microplate reader (Thermo Scientific Multi-Skan Go) at a sample wavelength of 570 nm and a reference wavelength of 630 nm. The EC_{50} values for GA, NB, and KU-32 were determined by performing nonlinear regression of the sigmoidal dose response curves using GraphPad Prism (version 6, GraphPad Software). To quantify any degree of synergy or antagonism between GA and either NB or KU-32, the CalcuSyn tool implementing the Chou–Talalay method (44) was used. Final DMSO concentrations were kept below 1% (v/v). All experiments were carried out in octuplicate.

Statistical analysis

All data are presented as mean ± S.D. from independent experiments. To determine whether the ATPase rates of Hsp90 in the presence of a combination of compounds were significantly different from the rates obtained in the presence of an individual compound, unpaired two-tailed *t* tests were carried out between two data groups, and one-way analysis of variance (ANOVA) was carried out between five independent groups. *t* tests were used to make comparisons between ATPase rates obtained in the presence of either GA or NB alone as compared with when they were combined. ANOVA was used to make comparisons between ATPase rates in the presence of GA alone, NB alone, and the two in combination. The same protocol was followed for combinations involving GA and KU-32. Unpaired two-tailed *t* tests were carried out to determine whether the binding affinities of ATP and ADP to the Hsp90–GA/NB/KU-32 complexes were significantly different from the binding affinities of ATP and ADP obtained in the presence of Hsp90 alone. Similar *t* tests were used to compare the binding affinities obtained when GA was titrated against the Hsp90–NB complex (and vice versa) with the binding affinities of GA and NB to Hsp90 alone. Similar comparisons were made between binding affinities obtained for KU-32 and GA titrated against the Hsp90–GA and Hsp90–KU-32 complexes respectively. Moreover, binding affinity of NB to the Hsp90–KU-32 complex was compared with the binding affinity of NB to Hsp90 alone. Finally, the binding affinity of ATP to the Hsp90–KU-32–ADP complex was compared with its binding affinity to Hsp90 alone.

To determine whether the effect on the viability of HeLa cells induced by a combination of two compounds (either GA/NB or GA/KU-32) was significantly different as opposed to compounds acting alone, unpaired two-tailed *t* tests and ANOVA were carried out between independent groups of data. *t* tests were used to make comparisons between EC_{50} values of compounds in combinations (C1–C6) and individual EC_{50} values of GA, NB, or KU-32. ANOVA was used to make comparisons between EC_{50} values of GA and NB when acting alone as compared with them acting in combination (C1–C3). The same protocol was followed for combinations involving GA and KU-32.

t tests were performed to determine whether EC_{50} values obtained for luciferase renaturation in the presence of NB and KU-32 alone were significantly different from EC_{50} values obtained when luciferase renaturation was studied in the presence of a combination of compounds involving either GA/NB or GA/KU-32.

The data were analyzed by built-in statistical analysis software in GraphPad Prism (version 6). p values < 0.01 were considered statistically significant for the cytotoxicity and ATPase assays, whereas p values < 0.05 were considered statistically significant for the isothermal titration calorimetry and luciferase renaturation studies.

Docking and molecular dynamics study of hHsp90β with small molecules

The amino acid sequence of Hsp90β was obtained from UniProtKB (accession ID P08238), and its structure was modeled using Modeler 9.17 (45). Individual domains were modeled using human Hsp90α crystal structures from PDB as listed in Table S5. The loop region (residues 210–270) joining the NTD to the MD was modeled separately (as there was no structure available in PDB for this region) to obtain an energy-minimized Hsp90β monomer. The Hsp90β dimer was modeled using an (experimentally solved) extended HtpG structure, which was kindly provided by Dr. Agard (46). The template was found to have 100% coverage with 39% identity and 59% similarity to the Hsp90β sequence. The structure was subjected to a short (5-ns) MD simulation for removing clashes and bad contacts using the AMBER version 14 suite (47).

Binding sites were known for all of the compounds except for KU-32, whose exact binding site at the CTD was to be determined. The rest were docked to facilitate subsequent MD simulations and confirm the accuracy of the modeled Hsp90β dimer. NB docked to the CTD of modeled hHsp90α (48) was used to model the binding site of NB at the CTD of the modeled Hsp90β dimer. The 3D structures of ATP and KU-32 were drawn using MarvinSketch followed by geometry optimization using Gaussian 9 (49), which utilized the B3LYP/6–31G* basis set. Additionally, RESP partial charges for all molecules were

calculated using Gaussian 9 software. NB, GA, and KU-32 structures thus obtained were docked to Hsp90β. Additionally, KU-32 was docked to the S532A/S586A mutant Hsp90β. All docking studies were performed using the ParDOCK (50) docking tool. Scoring was done using the BAPPL (51–53) scoring function. ATP docking to the modeled Hsp90β was further refined using the ATP-hHsp90α crystal structure (PDB 3T0Z). Two water molecules and one magnesium ion were added (as per the crystal structure) to each monomer of the modeled Hsp90β dimer. Distance between Mg^{2+}-coordinating atoms were kept between 2 and 2.2 Å in agreement with the crystal structure. Parameters for the final complex were prepared using MCPB (54) methodology and made available in AMBER version 14.

MD simulations were carried out using the AMBER version 14 (47) suite 5,6 on Nvidia K20 GPU cards at the Supercomputing Facility for Bioinformatics and Computational Biology (IIT Delhi, India). All of the Hsp90β–ligand complexes were solvated in cubic boxes of TIP3P (55) water molecules. The solvated complex was neutralized using Na^+ counterions. The study utilized periodic boundary conditions and PME summation (56) for electrostatic calculations. The shake (17) methodology was applied to restrict covalently bonded hydrogen atoms. Constant pressure conditions were realized using a Berenson thermostat (17). Time steps of 2 fs with 9-Å cut-off for nonbonded interactions were applied to the studies. Each system was energy-minimized using 250 steps of steepest descent followed by 750 steps of conjugate gradient. Heating to 300 K was done, keeping the protein-ligand complexes fixed with a force of 25 newtons. Equilibration was performed by simulating the structure while simultaneously decreasing the force on the protein–ligand complex in steps up to 0.1 newton. This was followed by a fully unrestricted equilibration of 5 ns at 300 K. Convergence of energy and density was monitored. Production was carried out for 420 ns for Hsp90β–KU-32, Hsp90β–ATP–KU-32, and S532A/S586A Hsp90β–KU-32 complexes, whereas all other ligand–protein complexes were subjected to 250 ns at NPT conditions.

Author contributions—T. K. C. and B. K. C. conceived the study. B. K. C. produced the proteins, performed the biochemical and cell-based studies, analyzed the data, and wrote the manuscript with the help of A. J. A. J. performed *in silico* studies, and A. J. and B. J. analyzed the data. B. K. C., V. K., and S. D. performed isothermal titration calorimetry experiments and analyzed the data. R. E. D. synthesized KU-32 under the supervision of B. B. T. K. C., R. E. D., and B. B. edited the manuscript and provided valuable suggestions to enhance the quality of the study and the manuscript.

Acknowledgments—B. K. C. and T. K. C. thank Prof. Johannes Buchner and Dr. William Kaelin Jr. for providing the Hsp90β and firefly luciferase plasmids, respectively, and for answering certain queries related to this work. The authors would also like to thank Jon Tally for carefully reading the manuscript and providing valuable suggestions. B. K. C. thanks Harsha Rohira and Ashutosh Pastor for constant support, encouragement, and technical advice. B. K. C., A. J., V. K., B. J., S. D., and T. K. C. thank the Indian Institute of Technology (Delhi, India) and Kusuma Trust for their financial support and for providing the infrastructure required to execute this project.

References

1. Taipale, M., Jarosz, D. F., and Lindquist, S. (2010) HSP90 at the hub of protein homeostasis: emerging mechanistic insights. *Nat. Rev. Mol. Cell Biol.* **11,** 515–528 CrossRef Medline
2. Lotz, G. P., Brychzy, A., Heinz, S., and Obermann, W. M. J. (2008) A novel HSP90 chaperone complex regulates intracellular vesicle transport. *J. Cell Sci.* **121,** 717–723 CrossRef Medline
3. French, J. B., Zhao, H., An, S., Niessen, S., Deng, Y., Cravatt, B. F., and Benkovic, S. J. (2013) Hsp70/Hsp90 chaperone machinery is involved in the assembly of the purinosome. *Proc. Natl. Acad. Sci. U.S.A.* **110,** 2528–2533 CrossRef Medline
4. Bagatell, R., and Whitesell, L. (2004) Altered Hsp90 function in cancer: a unique therapeutic opportunity. *Mol. Cancer Ther.* **3,** 1021–1030 CrossRef Medline
5. Xu, Y., Singer, M. A., and Lindquist, S. (1999) Maturation of the tyrosine kinase c-src as a kinase and as a substrate depends on the molecular chaperone Hsp90. *Proc. Natl. Acad. Sci. U.S.A.* **96,** 109–114 CrossRef Medline
6. Ahsan, A., Ramanand, S. G., Whitehead, C., Hiniker, S. M., Rehemtulla, A., Pratt, W. B., Jolly, S., Gouveia, C., Truong, K., Van Waes, C., Ray, D., Lawrence, T. S., and Nyati, M. K. (2012) Wild-type EGFR is stabilized by direct interaction with HSP90 in cancer cells and tumors. *Neoplasia* **14,** 670–677 CrossRef Medline
7. Xu, W., Yuan, X., Xiang, Z., Mimnaugh, E., Marcu, M., and Neckers, L. (2005) Surface charge and hydrophobicity determine ErbB2 binding to the Hsp90 chaperone complex. *Nat. Struct. Mol. Biol.* **12,** 120–126 CrossRef Medline
8. Müller, L., Schaupp, A., Walerych, D., Wegele, H., and Buchner, J. (2004) Hsp90 regulates the activity of wild type p53 under physiological and elevated temperatures. *J. Biol. Chem.* **279,** 48846–48854 CrossRef Medline
9. Pratt, W. B., and Toft, D. O. (2003) Regulation of signaling protein function and trafficking by the hsp90/hsp70-based chaperone machinery. *Exp. Biol. Med.* (*Maywood*) **228,** 111–133 CrossRef Medline
10. Daturpalli, S., Waudby, C. A., Meehan, S., and Jackson, S. E. (2013) Hsp90 inhibits α-synuclein aggregation by interacting with soluble oligomers. *J. Mol. Biol.* **425,** 4614–4628 CrossRef Medline
11. Maiti, P., Manna, J., Veleri, S., and Frautschy, S. (2014) Molecular chaperone dysfunction in neurodegenerative diseases and effects of curcumin. *Biomed. Res. Int.* **2014,** 495091 CrossRef Medline
12. Solárová, Z., Mojžiš, J., and Solár, P. (2015) Hsp90 inhibitor as a sensitizer of cancer cells to different therapies. *Int. J. Oncol.* **46,** 907–926 CrossRef Medline
13. Didenko, T., Duarte, A. M. S., Karagöz, G. E., and Rüdiger, S. G. D. (2012) Hsp90 structure and function studied by NMR spectroscopy. *Biochim. Biophys. Acta* **1823,** 636–647 CrossRef Medline
14. Donnelly, A., and Blagg, B. S. J. (2008) Novobiocin and additional inhibitors of the Hsp90 C-terminal nucleotide-binding pocket. *Curr. Med. Chem.* **15,** 2702–2717 CrossRef Medline
15. Marcu, M. G., Chadli, A., Bouhouche, I., Catelli, M., and Neckers, L. M. (2000) The heat shock protein 90 antagonist novobiocin interacts with a previously unrecognized ATP-binding domain in the carboxyl terminus of the chaperone. *J. Biol. Chem.* **275,** 37181–37186 CrossRef Medline
16. Soti, C., Vermes, A., Haystead, T. A. J., Csermely, P. (2003) Comparative analysis of the ATP-binding sites of Hsp90 by nucleotide affinity cleavage: a distinct nucleotide specificity of the C-terminal ATP-binding site. *Eur. J. Biochem.* **270,** 2421–2428 CrossRef Medline
17. Ryckaert, J. P., Ciccotti, G., and Berendsen, H. J. C. (1977) Numerical integration of the cartesian equations of motion of a system with constraints: molecular dynamics of *n*-alkanes. *J. Comput. Phys.* **23,** 327–341 CrossRef
18. Marcu, M. G., Schulte, T. W., and Neckers, L. (2000) Novobiocin and related coumarins and depletion of heat shock protein 90-dependent signaling proteins. *J. Natl. Cancer Inst.* **92,** 242–248 CrossRef Medline
19. Weikl, T., Muschler, P., Richter, K., Veit, T., Reinstein, J., and Buchner, J. (2000) C-terminal regions of Hsp90 are important for trapping the nucleotide during the ATPase cycle. *J. Mol. Biol.* **303,** 583–592 CrossRef Medline
20. Stebbins, C. E., Russo, A. A., Schneider, C., Rosen, N., Hartl, F. U., and Pavletich, N. P. (1997) Crystal structure of an Hsp90–geldanamycin complex: targeting of a protein chaperone by an antitumor agent. *Cell* **89,** 239–250 CrossRef Medline

21. Eskew, J. D., Sadikot, T., Morales, P., Duren, A., Dunwiddie, I., Swink, M., Zhang, X., Hembruff, S., Donnelly, A., Rajewski, R. A., Blagg, B. S. J., Manjarrez, J. R., Matts, R. L., Holzbeierlein, J. M., and Vielhauer, G. A. (2011) Development and characterization of a novel C-terminal inhibitor of Hsp90 in androgen dependent and independent prostate cancer cells. *BMC Cancer* **11,** 468 CrossRef Medline
22. Cohen, S. M., Mukerji, R., Samadi, A. K., Zhang, X., Zhao, H., Blagg, B. S. J., and Cohen, M. S. (2012) Novel C-terminal Hsp90 inhibitor for head and neck squamous cell cancer (HNSCC) with *in vivo* efficacy and improved toxicity profiles compared with standard agents. *Ann. Surg. Oncol.* **19,** Suppl. 3, S483–S490 CrossRef Medline
23. Zhao, H., Yan, B., Peterson, L. B., and Blagg, B. S. J. (2012) 3-Arylcoumarin derivatives manifest anti-proliferative activity through Hsp90 inhibition. *ACS Med. Chem. Lett.* **3,** 327–331 CrossRef Medline
24. Shelton, S. N., Shawgo, M. E., Matthews, S. B., Lu, Y., Donnelly, A. C., Szabla, K., Tanol, M., Vielhauer, G. A., Rajewski, R. A., Matts, R. L., Blagg, B. S. J., and Robertson, J. D. (2009) KU135, a novel novobiocin-derived C-terminal inhibitor of the 90-kDa heat shock protein, exerts potent antiproliferative effects in human leukemic cells. *Mol. Pharmacol.* **76,** 1314–1322 CrossRef Medline
25. Farmer, K., Williams, S. J., Novikova, L., Ramachandran, K., Rawal, S., Blagg, B. S. J., Dobrowsky, R., and Stehno-Bittel, L. (2012) KU-32, a novel drug for diabetic neuropathy, is safe for human islets and improves *in vitro* insulin secretion and viability. *Exp. Diabetes Res.* **2012,** 1–11 CrossRef Medline
26. Ansar, S., Burlison, J. A., Hadden, M. K., Yu, X. M., Desino, K. E., Bean, J., Neckers, L., Audus, K. L., Michaelis, M. L., and Blagg, B. S. J. (2007) A non-toxic Hsp90 inhibitor protects neurons from Aβ-induced toxicity. *Bioorganic Med. Chem. Lett.* **17,** 1984–1990 CrossRef Medline
27. Prodromou, C., Panaretou, B., Chohan, S., Siligardi, G., O'Brien, R., Ladbury, J. E., Roe, S. M., Piper, P. W., and Pearl, L. H. (2000) The ATPase cycle of Hsp90 drives a molecular "clamp" via transient dimerization of the N-terminal domains. *EMBO J.* **19,** 4383–4392 CrossRef Medline
28. Owen, B. A. L., Sullivan, W. P., Felts, S. J., and Toft, D. O. (2002) Regulation of heat shock protein 90 ATPase activity by sequences in the carboxyl terminus. *J. Biol. Chem.* **277,** 7086–7091 CrossRef Medline
29. Panaretou, B., Prodromou, C., Roe, S. M., O'Brien, R., Ladbury, J. E., Piper, P. W., and Pearl, L. H. (1998) ATP binding and hydrolysis are essential to the function of the Hsp90 molecular chaperone *in vivo*. *EMBO J.* **17,** 4829–4836 CrossRef Medline
30. Verba, K. A., Wang, R. Y., Arakawa, A., Liu, Y., Shirouzu, M., Yokoyama, S., and Agard, D. A. (2016) Atomic structure of Hsp90:Cdc37:Cdk4 reveals Hsp90 regulates kinase via dramatic unfolding. *Science* **352,** 1542–1547 CrossRef Medline
31. Li, J., Sun, L., Xu, C., Yu, F., Zhou, H., Zhao, Y., Zhang, J., Cai, J., and Mao, C. (2012) Structure insights into mechanisms of ATP hydrolysis and the activation of human heat-shock protein 90. *Acta Biochim. Biophys. Acta Sin.* (*Shanghai*) **44,** 300–306 CrossRef Medline
32. Colombo, G., Morra, G., Meli, M., and Verkhivker, G. (2008) Understanding ligand-based modulation of the Hsp90 molecular chaperone dynamics at atomic resolution. *Proc. Natl. Acad. Sci. U.S.A.* **105,** 7976–7981 CrossRef Medline
33. Hiss, D. C., Gabriels, G. A., and Folb, P. I. (2007) Combination of tunicamycin with anticancer drugs synergistically enhances their toxicity in multidrug-resistant human ovarian cystadenocarcinoma cells. *Cancer Cell Int.* **7,** 1–14 CrossRef Medline
34. Richter, K., Muschler, P., Hainzl, O., and Buchner, J. (2001) Coordinated ATP hydrolysis by the Hsp90 dimer. *J. Biol. Chem.* **276,** 33689–33696 CrossRef Medline
35. Cunningham, C. N., Krukenberg, K. A., and Agard, D. A. (2008) Intra- and intermonomer interactions are required to synergistically facilitate ATP hydrolysis in Hsp90. *J. Biol. Chem.* **283,** 21170–21178 CrossRef Medline
36. Zhang, H., Zhou, C., Chen, W., Xu, Y., Shi, Y., Wen, Y., and Zhang, N. (2015) A dynamic view of ATP-coupled functioning cycle of Hsp90 N-terminal domain. *Sci. Rep.* **5,** 9542 CrossRef Medline
37. Yu, X. M., Shen, G., Neckers, L., Blake, H., Holzbeierlein, J., Cronk, B., and Blagg, B. S. J. (2005) Hsp90 inhibitors identified from a library of novobiocin analogues. *J. Am. Chem. Soc.* **127,** 12778–12779 CrossRef Medline
38. Pratt, W. B., Gestwicki, J. E., Osawa, Y., and Lieberman, A. P. (2015) Targeting proteostasis through the protein quality control function of the Hsp90/Hsp70-based chaperone machinery for treatment of adult onset neurodegenerative diseases. *Annu. Rev. Pharmacol. Toxicol.* **55,** 353–371 CrossRef Medline
39. Lee, S. M., Chin, L. S., and Li, L. (2012) Protein misfolding and clearance in demyelinating peripheral neuropathies: therapeutic implications. *Commun. Integr. Biol.* **5,** 107–110 CrossRef Medline
40. Vital, A., Meissner, W. G., Canron, M. H., Martin-Negrier, M. L., Bezard, E., Tison, F., and Vital, C. (2014) Intra-axonal protein aggregation in the peripheral nervous system. *J. Peripher. Nerv. Syst.* **19,** 44–49 CrossRef Medline
41. Zhang, X., Li, C., Fowler, S. C., Zhang, Z., Blagg, B. S. J., and Dobrowsky, R. T. (2018) Targeting heat shock protein 70 to ameliorate c-Jun expression and improve demyelinating neuropathy. *ACS Chem. Neurosci.* **9,** 381–390 CrossRef Medline
42. Richter, K., Moser, S., Hagn, F., Friedrich, R., Hainzl, O., Heller, M., Schlee, S., Kessler, H., Reinstein, J., and Buchner, J. (2006) Intrinsic inhibition of the Hsp90 ATPase activity. *J. Biol. Chem.* **281,** 11301–11311 CrossRef Medline
43. Safran, M., Kim, W. Y., O'Connell, F., Flippin, L., Günzler, V., Horner, J. W., Depinho, R. A., and Kaelin, W. G. (2006) Mouse model for noninvasive imaging of HIF prolyl hydroxylase activity: assessment of an oral agent that stimulates erythropoietin production. *Proc. Natl. Acad. Sci. U.S.A.* **103,** 105–110 CrossRef Medline
44. Chou, T. C. (2010) Drug combination studies and their synergy quantification using the Chou-Talalay method. *Cancer Res.* **70,** 440–446 CrossRef Medline
45. Webb, B., and Sali, A. (2014) Comparative protein structure modeling using MODELLER. *Curr. Protoc. Bioinformatics* **47,** 5.6.1–32 CrossRef Medline
46. Krukenberg, K. A., Southworth, D. R., Street, T. O., and Agard, D. A. (2009) pH-dependent conformational changes in bacterial Hsp90 reveal a Grp94-like conformation at pH 6 that is highly active in suppression of citrate synthase aggregation. *J. Mol. Biol.* **390,** 278–291 CrossRef Medline
47. Case, D., Babin, V., Berryman, J., Betz, R., Cai, Q., Cerutti, D., Cheatham, 3rd, T., Darden, T., Duke, R., Gohlke, H., Goetz, A., Gusarov, S., Homeyer, N., Janowski, P., Kaus, J., *et al.* (2014) *Amber14 Reference Manual*, University of California, San Francisco
48. Matts, R. L., Dixit, A., Peterson, L. B., Sun, L., Voruganti, S., Kalyanaraman, P., Hartson, S. D., Verkhivker, G. M., and Blagg, B. S. J. (2011) Elucidation of the Hsp90 C-terminal inhibitor binding site. *ACS Chem. Biol.* **6,** 800–807 CrossRef Medline
49. Frisch, M., Trucks, G., Schlegel, H., Scuseria, G., Robb, M., Cheeseman, J., Scalmani, G., Barone, V., Petersson, G., Nakatsuji, H., Li, X., Caricato, M., Marenich, A., Bloino, J., Janesko, B., *et al.* (2016) *Gaussian 16 Revision A.03*, Gaussian, Inc., Wallingford CT
50. Gupta, A., Gandhimathi, A., Sharma, P., and Jayaram, B. (2007) ParDOCK: an all atom energy based Monte Carlo docking protocol for protein-ligand complexes. *Protein Pept. Lett.* **14,** 632–646 CrossRef Medline
51. Jain, T., and Jayaram, B. (2005) An all atom energy based computational protocol for predicting binding affinities of protein-ligand complexes. *FEBS Lett.* **579,** 6659–6666 CrossRef Medline
52. Jain, T., and Jayaram, B. (2007) Computational protocol for predicting the binding affinities of zinc containing metalloprotein–ligand complexes. *Proteins* **67,** 1167–1178 CrossRef Medline
53. Singh, T., Adekoya, O. A., and Jayaram, B. (2015) Understanding the binding of inhibitors of matrix metalloproteinases by molecular docking, quantum mechanical calculations, molecular dynamics simulations, and a MMGBSA/MMBappl study. *Mol. BioSyst.* **11,** 1041–1051 CrossRef Medline
54. Li, P., and Merz, K. M. (2016) MCPB.py: a Python based metal center parameter builder. *J. Chem. Inf. Model.* **56,** 599–604 CrossRef Medline
55. Jorgensen, W. L., Chandrasekhar, J., Madura, J. D., Impey, R. W., and Klein, M. L. (1983) Comparison of simple potential functions for simulating liquid water. *J. Chem. Phys.* **79,** 926–935 CrossRef
56. Berendsen, H. J. C., Postma, J. P. M., van Gunsteren, W. F., DiNola, A., and Haak, J. R. (1984) Molecular dynamics with coupling to an external bath. *J. Chem. Phys.* **81,** 3684–3690 CrossRef